



저작자표시-비영리-변경금지 2.0 대한민국

이용자는 아래의 조건을 따르는 경우에 한하여 자유롭게

- 이 저작물을 복제, 배포, 전송, 전시, 공연 및 방송할 수 있습니다.

다음과 같은 조건을 따라야 합니다:



저작자표시. 귀하는 원저작자를 표시하여야 합니다.



비영리. 귀하는 이 저작물을 영리 목적으로 이용할 수 없습니다.



변경금지. 귀하는 이 저작물을 개작, 변형 또는 가공할 수 없습니다.

- 귀하는, 이 저작물의 재이용이나 배포의 경우, 이 저작물에 적용된 이용허락조건을 명확하게 나타내어야 합니다.
- 저작권자로부터 별도의 허가를 받으면 이러한 조건들은 적용되지 않습니다.

저작권법에 따른 이용자의 권리는 위의 내용에 의하여 영향을 받지 않습니다.

이것은 [이용허락규약\(Legal Code\)](#)을 이해하기 쉽게 요약한 것입니다.

[Disclaimer](#)

# Optimization of Full Cell Formulation Factors Based on Silicon – Graphite Composite Negative Electrode



Sung Won Jung

Battery Science and Technology program  
Graduate School of UNIST

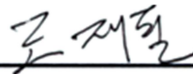
# Optimization of Full Cell Formulation Factors Based on Silicon – Graphite Composite Negative Electrode

A thesis  
submitted to the Graduate School of UNIST  
in partial fulfillment of the  
requirements for the degree of  
Master of Science

Sung Won Jung

2. 8. 2013

Approved by



---

Major Advisor

[Jaephil Cho]

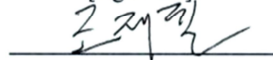
# Optimization of Full Cell Formulation Factors Based on Silicon – Graphite Composite Negative Electrode

Sung Won Jung

This certifies that the thesis of Sung Won Jung is approved.

2. 8. 2013

[signature]



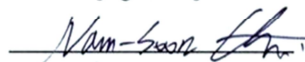
Thesis supervisor: [Jaephil Cho]

[signature]



[Sang-Young Lee]

[signature]



[Nam-Soon Choi]



## Contents

Abstract.....	5
Figures and table.....	6
I. INTRODUCTION.....	10
1.1 Full cell capacity	
1.2 Silicon for negative electrode material	
1.3 Natural graphite for negative electrode material	
1.4 Binder for silicon based negative electrode	
1.5 Electrolyte	
1.6 Design of full cell capacity	
II. EXPERIMENT.....	23
2.1 Materials	
2.2 Electrochemical measurement	
2.3 Instrumental analysis	
III. RESULTS AND DISCUSSIONS.....	24
3.1 Particle size effect of natural graphite	
3.2 Design for cutoff voltage in a full cell	
3.3 Design for initial discharge capacity in a full cell	
3.4 Optimization of binder and electrolyte	
IV. CONCLUSION.....	40
V. REFERENCES.....	42
VI. Thanks to.....	44

## Abstract

In the state of the art progress in improving the performance of the Lithium Ion Batteries (LIB) full cell, the formulation engineering has received little attention, compared to new structures and new compositions of the electrochemically active material so far. However, much attention is paid to the formulation engineering in the field of battery industry, because it is critically significant in order to manufacture efficient full cells which can be commercialized. Such efforts are quite restricted to access or publication, because they are the proprietary information of the manufacturing companies.

This study is focused on the optimization of full cell formulation factors based on silicon-natural graphite composite negative electrode. The considered factors were composition of active materials, binder, electrolyte and cutoff voltage in a full cell.

The effect of different particle sizes of natural graphite within the composite, which is composed of silicon and natural graphite, was investigated, in which the composite with smaller natural graphite showed the superior electrical conductive network.

The experiment showed that the silicon based composite electrode keeps higher voltage profile than that of natural graphite, especially during delithiation in the half cell. And, the simulation result, computed out of the experimental result, envisioned that it is better to shift cutoff voltage to the lower voltage during discharge in the full cell consisting of silicon–natural graphite composite electrode in order to use the maximum capacity of each electrode, comparing with that of natural graphite electrode. Additionally, a design method of calculating initial discharge capacity in a full cell was investigated.

A statistical analysis method making use of Design of Experiments (DOE) was applied to search for the optimized condition for the weight ratio of binder mixture and the electrolyte kind, which showed that the cycle life of silicon-natural graphite composite electrode with the PAA or CMC binders is superior to that with SBR binder. This experimental result enabled me to argue that those binders, which have mechanically high ‘proportional limit stress’ like PAA and CMC, provide more robust bonds among expansive active materials (Si) which, in turn, can be adhered solidly to current collector substrate, compared with SBR and PVDF which have low ‘proportional limit stress’. Such strong bonds are also formed even between Si and Natural graphite of active materials, which contributed to the preservation of electrical conductivity of a composite negative electrode despite under repeated dimensional changes during cycles.

## Figure captions

**Figure 1.** Estimate of total capacity of the LIB material a) as a function of the cathode specific capacity and b) as a function of the anode specific capacity.

**Figure 2.** Upper: schematic illustration of the preparation of macro porous Si powders. Ag nano particles were deposited onto the surface of bulk silicon via a galvanic reaction, and subsequently, the Ag-deposited Si was chemically etched to make 3D porous Si particles. Lower: a) SEM image of Ag deposited Si, b) SEM image of chemically etched Si, c) magnified SEM image of samples seen in (b).

**Figure 3.** Electrochemical evaluation of the carbon-coated porous Si: a) voltage profiles of the carbon-coated porous Si anodes between 0.005 and 1.2 V in a coin-type half cell at 0.1 C rate (the first cycle) and 0.2 C (2nd–50th cycles) in the same conditions, b) plot of charge capacity vs. cycle number obtained from voltage profiles seen in (a), and, c) rate capabilities of the carbon-coated porous Si anodes.

**Figure 4.** Voltage profiles of the natural graphite (red solid line) and the porous Si negative electrodes (blue dotted line) at 0.1C rate in coin type half-cell. Plot of voltage versus (a) the specific capacity and (b) the normalized capacity of each electrode.

**Figure 5.** a) Schematic views of the raw natural graphite flakes, b) various shaped natural graphite and c) the shuttle-shaped natural graphite.

**Figure 6.** Stress-strain diagrams of a) CMC and PVDF and b) typical brittle material ( $\sigma$ :stress,  $\epsilon$ :strain) with proportional limit(point A) and fracture stress(point B).

**Figure 7.** a) PAA and CMC before condensation, b) Cross-linked binder after condensation and c) chemical bonding between silicon and cross-linked binder.

**Figure 8.** Schematic view of transportation of the solvated lithium ions between two electrodes.

**Figure 9.** Molecular structure of organic carbonates solvents.

**Figure 10.** Graphical views of the full cell capacity design: a) initial charge voltage profile of cathode half cell(above) and initial discharge voltage profile of anode(below) b) after loading balance

(N/P=1.2) c) simulation of initial charge voltage profile of the full cell d) normalized capacity with charging cutoff voltage 4.2 V.

**Figure 11.** Schematic views of a full cell capacity a) each reversible and irreversible capacity of cathode and anode half cell, b) charging capacity of a full cell and c) discharging capacity of a full cell.

**Figure 12.** SEM image of (a) shuttle-shaped natural graphite, (b) spherical natural graphite and (c) porous silicon.

**Figure 13.** Initial discharge-charge voltage profiles (red solid line) of porous Si and shuttle-shaped natural graphite composite and (blue dotted line) of porous Si and spherical natural graphite composite.

**Figure 14.** Electrode morphology of (a) porous Si and spherical natural graphite composite, (b) magnified SEM image of samples seen in (a), (c) porous Si and Shuttle-shaped natural graphite composite, (d) magnified SEM image of samples seen in (c), (e) nano-sized Si and shuttle-shaped natural graphite composite and (f) magnified SEM image of samples seen in (e).

**Figure 15.** Schematic diagrams of (a) Si/spherical natural graphite composite and (b) Si/shuttle-shaped natural graphite composite.

**Figure 16.** (a) Half-cell specific capacity-voltage profiles of natural graphite (black dotted line) and porous Si/natural graphite composite (red solid line), (b) half-cell normalized capacity-voltage profiles of natural graphite (black dotted line) and porous Si/natural graphite composite (red solid line), (c) half-cell normalized discharge capacity-voltage profiles of LiCoO<sub>2</sub> (black solid line), natural graphite (red solid line) and porous Si/natural graphite composite (blue solid line), (d) full cell normalized discharge capacity-voltage profiles of LiCoO<sub>2</sub>-natural graphite (black solid line) and LiCoO<sub>2</sub>-porous Si/natural graphite composite (red solid line).

**Figure 17.** Three electrode pictures of (a) LiCoO<sub>2</sub> positive electrode(left) and Si/natural graphite negative electrode(right), (b) negative electrode wrapped with separator, (c) Li metal reference electrode placed between positive electrode and negative electrode and (d) pouch type three electrode.

**Figure 18.** Three electrode voltage profiles of LiCoO<sub>2</sub> positive electrode voltage profile(upper) , full cell voltage profile(middle) and Si/ShNG negative electrode(below); (a) actual three electrode

voltage profiles, (b) three electrode voltage profiles (simulated positive electrode voltage profile is substituted with actual positive electrode voltage profile).

**Figure 19.** Main effect plots of (a) initial specific discharge capacity and (b) initial coulombic efficiency.

**Figure 20.** Schematic diagram of plastic deformation and elastic deformation.

**Figure 21.** Full cell cycle life with normalized capacity after 0.1 C formation (0.5 C charging, 1 C discharging, 4.2~2.5 V cutoff).

**Figure 22.** Full cell cycle life with normalized capacity after 0.1 C formation:  
(red solid line) LiCoO<sub>2</sub>/spherical natural graphite, (blue solid line) LiCoO<sub>2</sub>-porous Si/shuttle-shaped natural graphite with PAA and CMC binder, and (black solid line) LiCoO<sub>2</sub>-porous Si/shuttle-shaped natural graphite with SBR and CMC binder.

## **Table captions**

**Table 1.** Properties of electrolyte solvents.

**Table 2.** Active materials for negative electrode used in experiments and providers of them.

**Table 3.** Composition of negative electrode and its wt %

**Table 4.** Electrolytes used in experiments.

**Table 5.** Particle diameter and specific surface area of each active material

**Table 6.** Design and actual values of full cell capacity.

**Table 7.** Factorial design of suspicious factors on the cell performance.

**Table 8.** Full factorial design and its results.

**Table 9.** Analysis of variance for initial specific discharge capacity and coulombic efficiency.

**Table 10.** Cycle life of the full cell made of different electrolyte and weight ratio of binder mixture.

# I. Introduction

## 1.1 Full cell capacity

A natural graphite has advantages like a flat and low voltage profile, high reversible capacity (370 mAh/g) and low cost. These advantages enabled a natural graphite to be widely used as a negative electrode material in lithium ion batteries (LIB) so far. Due to high demands of the materials with higher energy density which catch up with the development of mobile instruments, electrically-drive tools and electric vehicles, new negative electrode materials have been extensively investigated until now. To increase the energy density in lithium-ion batteries, naturally, increase of the capacities of a positive electrode material is more important than that of a negative electrode. Unfortunately, the maximum usage specific capacity of the positive electrode material has been limited to about 170 mAh/g even today.

Even so, according to the following equation, the needs for the improvement on the specific capacity of a negative electrode material should not be underestimated.

$$\text{Full cell specific capacity} = \frac{C_C}{1 + \frac{C_C}{C_A}} = \frac{C_A C_C}{C_A + C_C} (\text{mAhg}^{-1}) \quad [1] \text{-----(1)}$$

Full cell specific capacity: Total capacity

$C_A$  : negative electrode(anode) specific capacity.

$C_C$  : positive electrode(cathode) specific capacity

Making use of equation (1), the values of full cell specific capacity (mAh/g) can be plotted against the changes of a specific capacity (mAh/g) of each electrode, with either cathode or anode specific capacity is fixed. Fig. 1 (a) shows that the full cell specific capacity increases linearly with the increase of cathode specific capacity on the assumption that the specific capacity of a negative electrode made from commercialized natural graphite is fixed at 370 mAh/g; whilst, with the specific capacity of a positive electrode made from  $\text{LiCoO}_2$  is fixed at 140 mAh/g, the full cell specific capacity increases linearly up to 122 mAh/g as negative electrode specific capacity increase from the beginning to 1000 mAh/g, and then the full cell specific capacity increases slowly up to 135 mAh/g as a negative electrode specific capacity increases from 1000 to 4000 mAh/g, as shown in Fig. 1 (b). For this reason, the negative electrode material which showed larger specific capacity than a natural graphite is widely researched. Especially, silicon is mostly studied due to its high specific capacity.

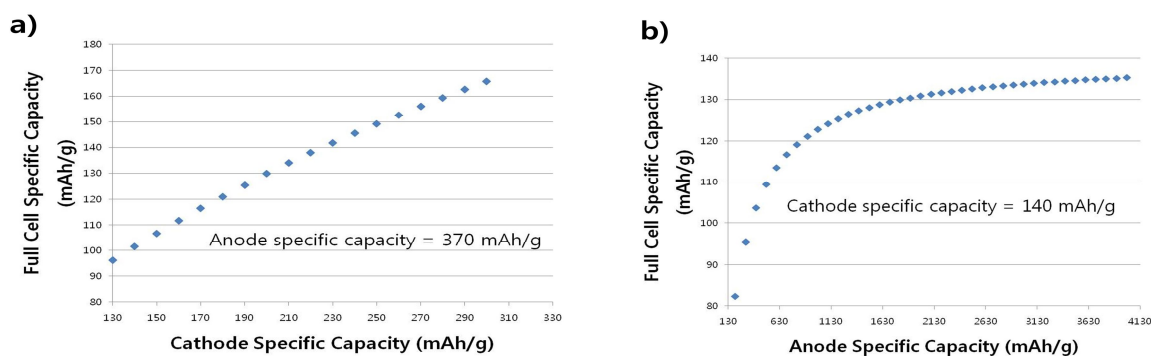


**Figure 1.** Estimate of total capacity of the LIB material a) as a function of the cathode specific capacity and b) as a function of the anode specific capacity.

### 1.2 Silicon for a negative electrode material

Metal elements that can alloy with lithium have attracted great attention because of the high theoretical capacity of individual element (e.g., Si: 4200 mA h/ g , Ge: 1600 mA h/ g , Sn: 990 mA h/ g , Sb: 660 mA h/ g ). Especially, silicon has been widely studied as one of the strongest negative electrode candidates, because it has 10 times higher gravimetric capacity (3579 mA h/g for  $\text{Li}_{15}\text{Si}_4$ ) and  $\sim 2$  times larger volumetric capacity ( $8322 \text{ mAh/cm}^3$ ) than carbonaceous negative electrodes.

However, despite the high theoretical specific capacity of silicon compared with graphite, its commercial use is still limited due to its severe volume change (300 %) during charge-discharge cycling and low electrical conductivity ( $6.7 \times 10^{-4} \text{ Scm}^{-1}$ ). In order to overcome the problematic stress that comes from volume change in silicon, there has been a wide range of studies on controlling the morphologies of silicon particles i.e. Si nanowire [2] , Si nanotube[3] and 3D porous Si[4, 5].

As anode materials, nano-sized silicons, such as nanowires and nanotubes, relieve geometrically the mechanical stress induced by the large volume change, and the porous-structured silicon also alleviates the volume change, while enhancing the rate capability of electrodes via shortened diffusion paths and increased surface area [6, 7]. For example, Bang et al. introduced the synthesis of 3D porous Si structure by way of silver(Ag) deposition and chemical etching, in which, galvanic reaction occurred causing Ag nano particles to deposit on the surface of silicon, when the bulk silicon particles are immersed into the mixture of hydrofluoric acid (HF) and  $\text{AgNO}_3$ . Then, when the Ag-deposited silicons are immersed into the etchant (HF + 2%  $\text{H}_2\text{O}_2$ ), the 3D macroporous silicon structure comes into being with the assistance of chemical etching, as has been described in Fig. 2.



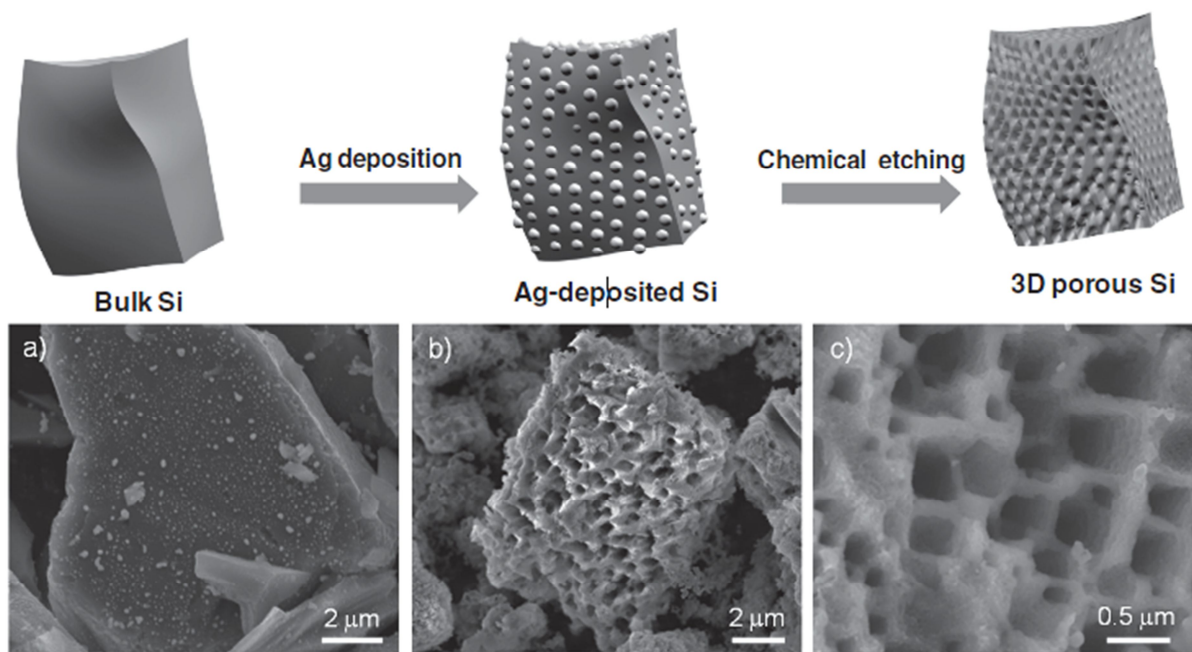


**Figure 2.** Upper: schematic illustration of the preparation of macro porous Si powders. Ag nano particles were deposited onto the surface of bulk silicon via a galvanic reaction, and subsequently, the Ag-deposited Si was chemically etched to make 3D porous Si particles. Lower: a) SEM image of Ag deposited Si, b) SEM image of chemically etched Si, c) magnified SEM image of samples seen in (b). Figure taken with permission[5]

Fig. 3 describes electrochemical evaluation of 3D porous silicon which was coated with carbon to improve the electrical conductivity. The specific capacity was the first discharge of 2530 mAh/g and charge capacities of 2390 mAh/g. The initial coulombic efficiency was 94.4 %. (Fig. 3)

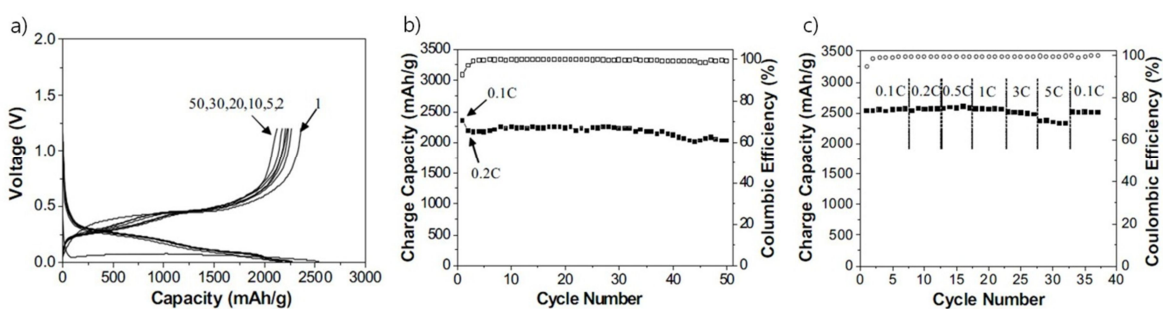


**Figure 3.** Electrochemical evaluation of the carbon-coated porous Si: a) voltage profiles of the carbon-coated porous Si anodes between 0.005 and 1.2 V in a coin-type half cell at 0.1 C rate (the first cycle) and 0.2 C (2nd–50th cycles) in the same conditions, b) plot of charge capacity vs. cycle number obtained from voltage profiles seen in (a), and, c) rate capabilities of the carbon-coated porous Si anodes. Figure taken with permission[5]

### 1.3 Natural graphite for a negative electrode material

To fabricate the silicon based negative electrode, blending silicon particles with the commercialized natural graphite is the first option because the complex conditions for the synthesis of active material leads to increase the production process and the cost of production. So, it is necessary to understand simultaneously the characteristics of both silicon and commercialized natural graphite. First of all, natural graphite is shown to be quite reversible during the intercalation and deintercalation of  $\text{Li}^+$  ion, as shown in Fig. 4 (a). Fig. 4 (a) show voltage profiles (Voltage vs. Specific capacity) of the natural graphite (red solid line) and the porous Si negative electrodes (blue dotted line) at 0.1C rate in coin type half-cell. Fig. 4 (b) shows the normalized capacity - voltage profiles from Fig. 4 (a), in which both materials show similar voltage plateaus during discharge (lithiation), while the curve of natural graphite shows better reversibility and is more flat and lower voltage than that of porous silicon especially during charge (delithiation).

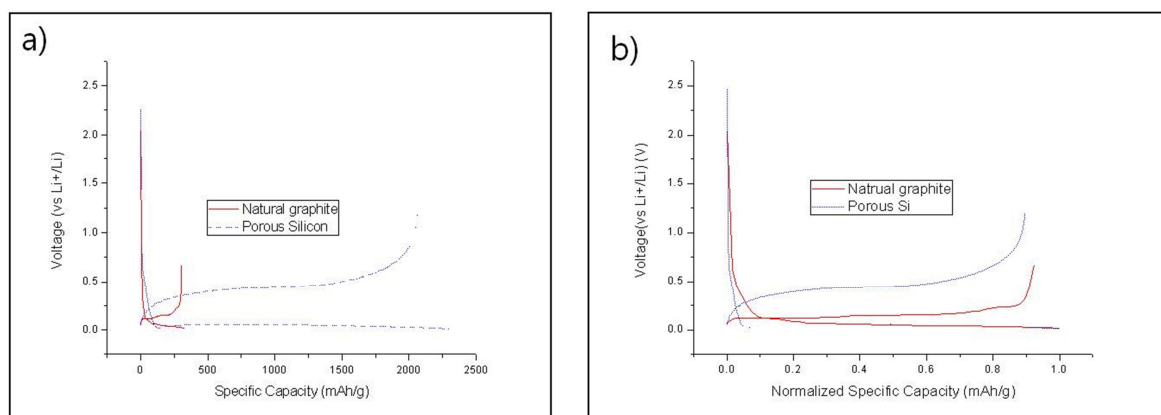


**Figure 4.** Voltage profiles of the natural graphite (red solid line) and the porous Si negative electrodes (blue dotted line) at 0.1C rate in coin type half-cell. Plot of voltage versus (a) the specific capacity and (b) the normalized capacity of each electrode.

In addition, it is well known that the electrical conductivity of a natural graphite ( $10^2\sim 10^4$  S/cm) is superior to that of silicon ( $10^{-4}$  S/cm). For this reason, silicon is usually applied as a form of composite with carbon in order to overcome the low conductivity of silicon. [1, 8] Despite its high conductivity, natural graphite has two major drawbacks during application; i) the first drawback is that the natural graphite is so sensitive to PC (Propylene carbonate)-based electrolytes, so that it is easily exfoliated in electrolytes, causing PC to decompose even into the explosion of propylene gas. As a way of overcoming this problem, EC (ethylene carbonate) is used as an alternative electrolyte, which prevents graphite from disintegrating physically at 0.8 V by forming an effective protective film (SEI). However, the EC electrolyte solvent alone cannot be used, because of its high melting point ( $\sim 36$  °C), so that an electrolyte solvent is used as a mixture with other electrolytes [9], ii) and the other

drawback is that the morphology of natural graphite flake is very anisotropic with thinner edge plane than basal planes, which makes it difficult for graphite slurry to spread uniformly. The schematic diagram of Fig. 5 (a) shows that the basal planes of the natural graphite flake particles, while coated on the current collector substrate, are exposed to the flow of  $\text{Li}^+$  diffusion, making it difficult for  $\text{Li}^+$  ion to intercalate and de-intercalate via the edge plane. This explains the bad rate capacity of the cell made from unmodified natural graphite. There have been quite a few researches to modify the morphology of the natural graphite and overcome the problematic issues that come from the intrinsic characteristic of natural graphite, anisotropy. Among different types of morphologically modified natural graphites shown in Fig. 5 (b), Fig. 5 (c) shows the shuttle-shaped natural graphite particles, which are stacked on the current collector substrate, with edge planes oriented at random.[10]

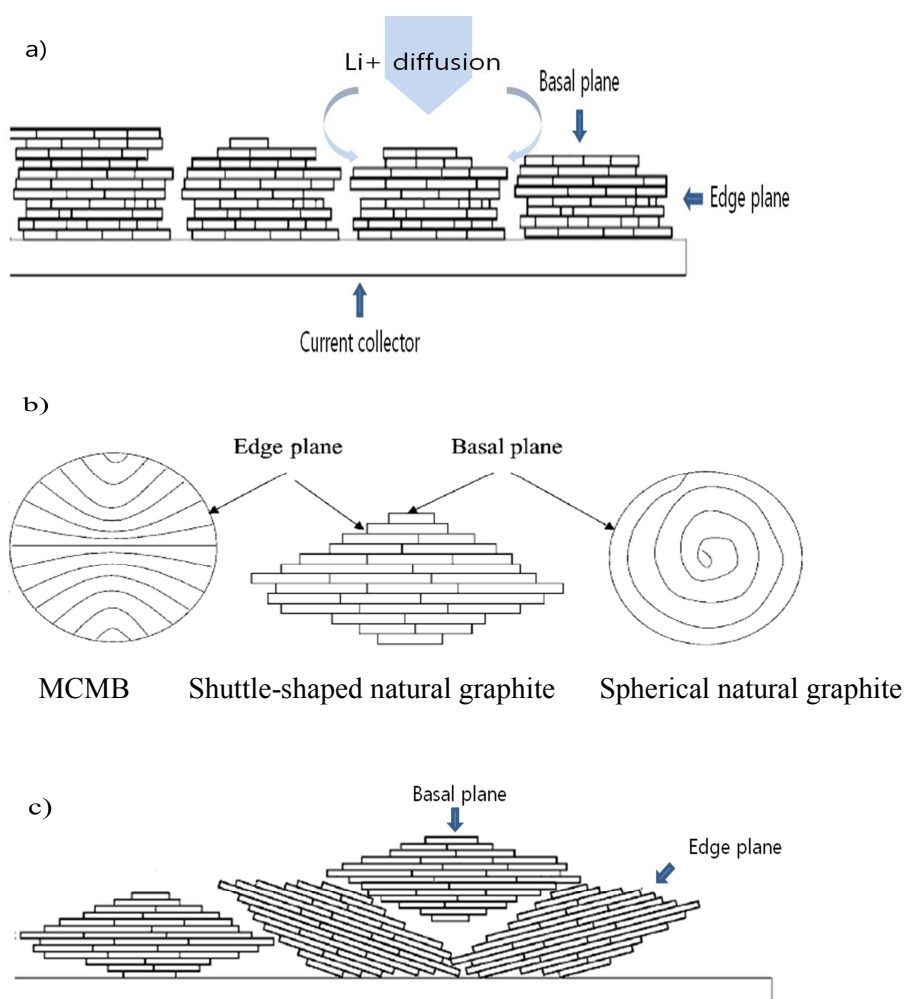


**Figure 5.** a) Schematic views of the raw natural graphite flakes, b) various shaped natural graphite and c) the shuttle-shaped natural graphite.

#### 1.4 Binder for a silicon based negative electrode

The optimization of binder to be used in electrode formulation engineering attract greater attention

in recent days, because the well-structured electrode formulation engineering with optimized binder condition is indispensable in designing new electrode material systems. Primarily, binder plays the role of binding coherently between active materials and conductive additives as a composite, which in turn adheres to current collector, and eventually enables the electrode to keep up electric conductivity despite repeated dimensional changes of the cell during long cycles. Binder also works as a dispersant agent, minimizing the agglomeration of each particle, which is a cause of capacity deterioration. [11] Among those commercialized binders, Poly(vinylidene fluoride) (PVdF), Styrene Butadiene Rubber (SBR), and sodium carboxymethyl cellulose (CMC) binder, SBR and CMC are soluble in aqueous, relatively cheaper and more eco-friendly than the conventional binder, polyvinylidene fluoride(PVDF), which uses poisonous N-Methyl-2-pyrrolidone (NMP) as a solvent. Besides, Dahn et al. reported that even the cycle life of silicon-based electrode differs greatly according to the application of different binders, showing superiority in the order of CMC, a mixture of CMC and SBR, and then PVDF. The excellence of applying CMC as a binder was not fully explained despite its high stiffness considering that the volume change of silicon particles upon lithiation can be up to 300%. [12]

It is generally accepted that binder should be very deformable to be used in silicon-based composite electrode, like PVDF and SBR, while CMC has a small elongation (brittle) before fracture, as compared in the stress-strain diagram of Fig. 6 (a). Fig. 6 (b) shows the typical stress-strain diagram for a brittle material, as indicated in CMC. This explains that not the mechanical deformation capacity of binder but the nature of the bonding is a key factor that determines the performance of a binder.[12, 13]

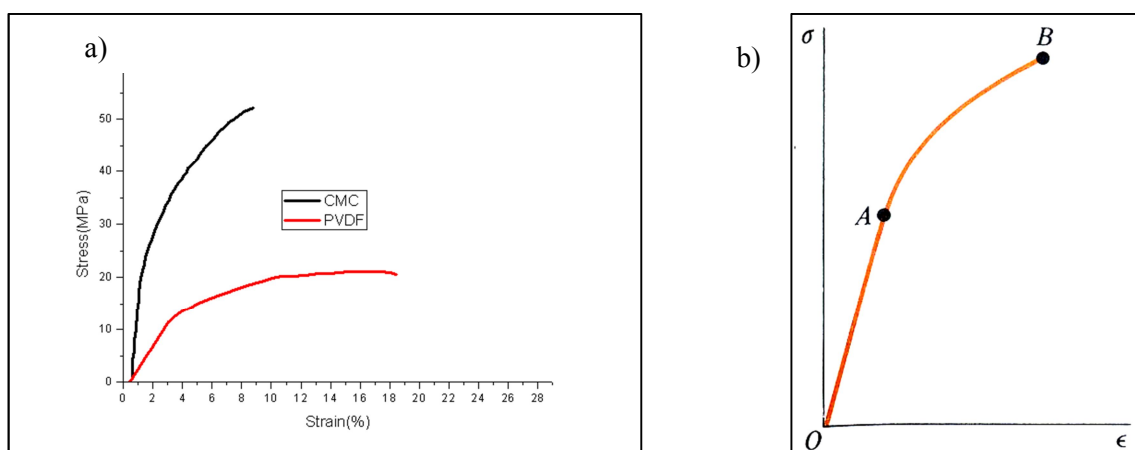


**Figure 6.** Stress-strain diagrams of a) CMC and PVDF and b) typical brittle material ( $\sigma$ :stress,  $\epsilon$ :strain) with proportional limit(point A) and fracture stress(point B).

There are some reports that both the chemical bonding and the mechanical bonding are contributive to the sustaining of the cell structure.[13, 14] Bridel et al. reported that a self-healing process of Si-

CMC hydrogen bonding through breaking and reforming bounds enables the structure to endure the structural stress during the repeated cycle.[13]. Recently, there is a report that the composite made from CMC and poly acrylic acid (PAA) provide better cyclic performance than others made from silicon based electrodes. Especially, Choi et al. proved that covalent ester bonds are formed by the condensation reaction (dehydration) between chemically cross-linked polymers (CMC and PAA) and silicon particles, which enables the structure to expand and absorb high mechanical stress when the  $\text{Li}^+$  is uptaken into Si.[14] Fig. 7 describes the schematic diagram of condensation reaction between the carboxylic acid groups of PAA and the hydroxyl groups of CMC occurring at 150 °C under vacuum into ester groups, during which the anhydride can be generated in a PAA chains.

There is also another condensation reaction between the free carboxylic acid of a PAA and the hydroxyl groups of the  $\text{SiO}_2$  layer on the silicon surface to form covalent ester bonds between the binder and the silicon as shown in Fig. 7.

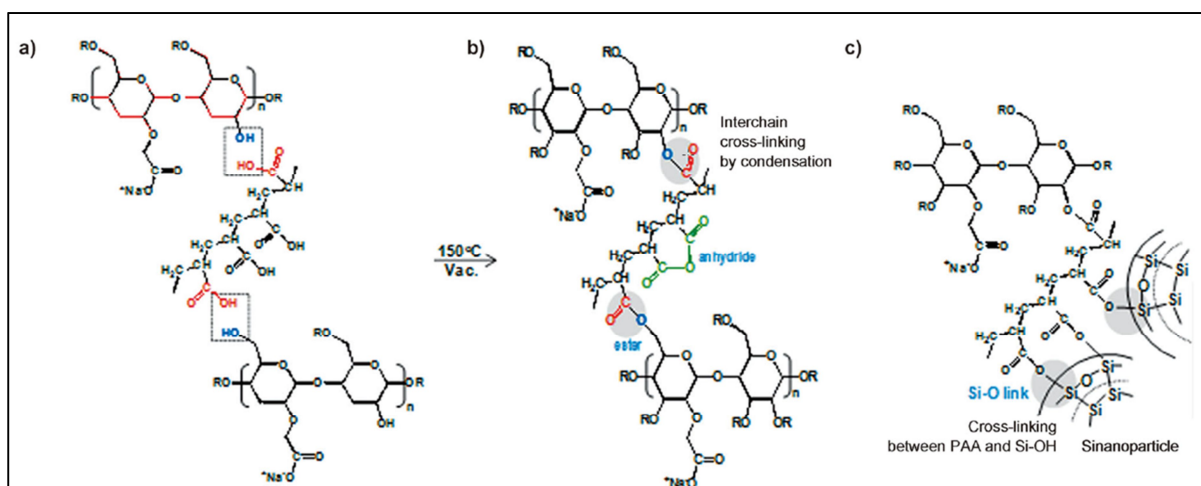


**Figure 7.** a) PAA and CMC before condensation, b) Cross-linked binder after condensation and c) chemical bonding between silicon and cross-linked binder. Figure taken with permission.[14]

### 1.5 Electrolyte

As an ionic conductor which transports ions from one electrode to the other within a cell, an electrolyte should meet the following properties: i) a good ionic conductor and electronic insulator minimizing self-discharge, ii) a wide electrochemical window to minimize electrolyte degradation, iii) inertness to other cell components, iv) a robustness against various abuses, such as electrical, mechanical or thermal stresses, and v) an environmental friendliness.[9] Non-aqueous liquid electrolyte, the most typical electrolyte, consists of  $\text{Li}^+$  salt and organic solvent, in which  $\text{Li}^+$  salt dissolves and dissociates by organic solvent which is composed of polar solvent molecules. The solvated  $\text{Li}^+$  ions with small ionic radius,  $0.7\text{\AA}$ , attached to no more than four solvent molecules,

move to the other electrode within the solvent media, as described in Fig. 8, during which the interfaces between the electrolyte and the two electrodes are often decisive in the performance of the cell.

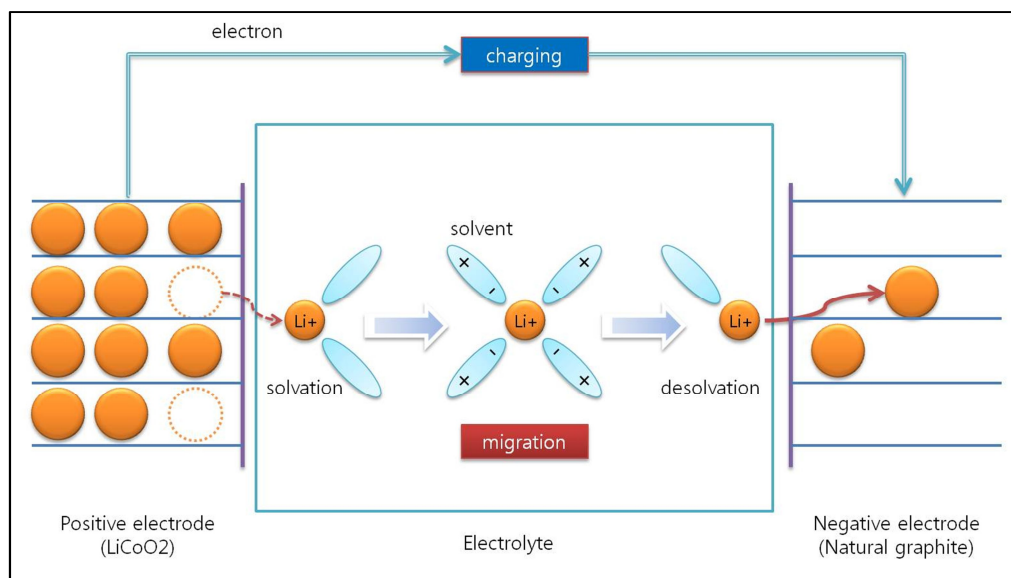


**Figure 8.** Schematic view of transportation of the solvated lithium ions between two electrodes.

Ionic conductivity in electrolyte is correlated with two factors; i) one is the dissolving ability of organic solvents, expressed as the dielectric constant, and ii) the other is ionic mobility denoting the migration ability of the solvated ions through the solvent media.

Ionic mobility ( $m$ ) can be expressed with Nernst-Einstein equation as shown in equation (2).

$$m = zeD/KT \text{ -----(2)}$$

$m$ : ionic mobility

$z$ : ionic charge

$e$ : magnitude of the charge of an electron.

$D$ : diffusion coefficient

$K$ : Boltzman's constant

$T$ : temperature

Diffusion coefficient ( $D$ ) correlated with the viscosity of the solvent can be expressed as Stokes-Einstein equation in equation (3)

$$D = KT/6\pi r\eta \text{ -----(3)}$$

r: radius of solvated ions

$\eta$ : viscosity

By combining Equation 2 and Equation 3, ionic mobility against viscosity can be expressed as equation (4).

$$\text{Ionic mobility: } m = ze/6\pi r\eta \text{ -----( 4)}$$

The inverse proportionality of ionic mobility against viscosity, as shown in equation (4), signifies that a good ionic conductive electrolyte requires that the solvent should have low viscosity and high dielectric constant. In order to overcome the drawback of each solvent, a mixture of different solvents usually works more efficiently than a single solvent. The dielectric constants and viscosities of several solvents, which are composed of organic carbonate, are listed in Table 1, which are divided into two groups according to molecular structure, cyclic and linear compounds, as described in Fig. 9.

**Table 1. Properties of electrolyte solvents [9]**

Solvent	Viscosity (25 °C) (cP)	Dielectric constant (25 °C)	Ionic conductivity (S/cm)
EC	1.90 (40 °C)	89.78	7.2
PC	2.53	64.92	5.8
DMC	0.59 (20 °C)	3.107	7.1
DEC	0.75	2.805	4.6
EMC	0.65	2.958	3.1



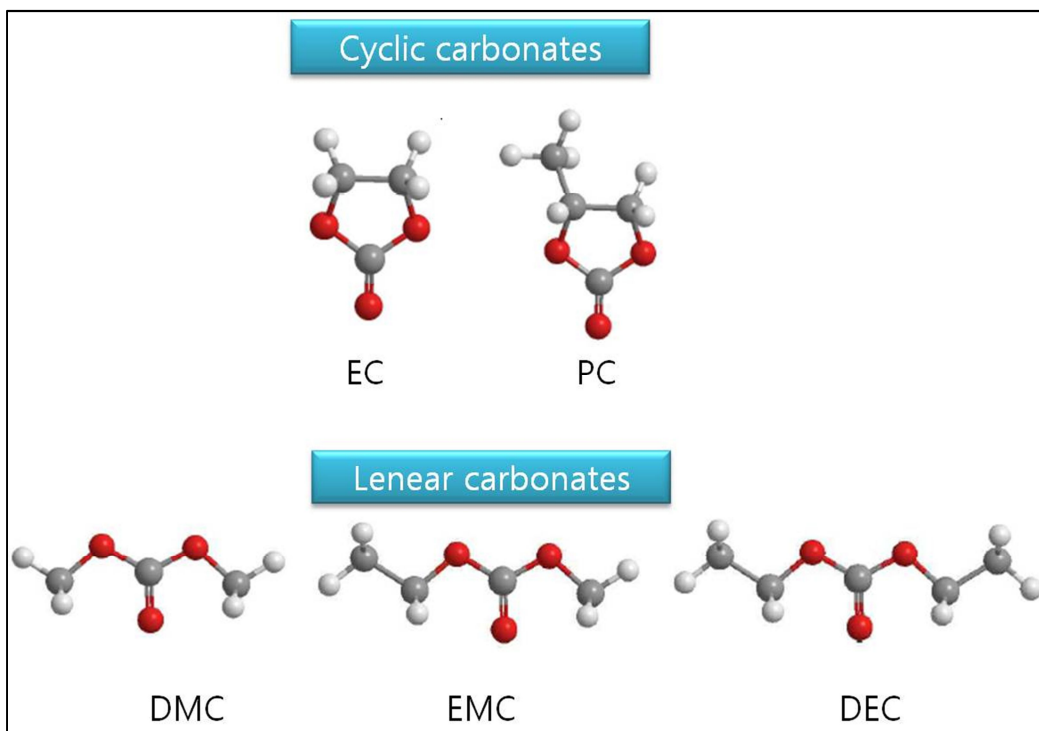


**Figure 9.** Molecular structure of organic carbonates solvents.

### 1.6 Design of a full cell capacity

We can design initial capacity of the full cell by combining the initial charge-discharge half-cell data of each electrode, as has been exemplified in Fig. 10 (a), in which the upper line is the charge (deintercalation) voltage profile of the  $\text{LiCoO}_2$  positive electrode, which is cut-off at 4.3 V, while the lower line is the discharge (intercalation) voltage profile of the natural graphite negative electrode, which is cutoff at 0.01 V. The specific capacity of the  $\text{LiCoO}_2$  positive electrode and the natural graphite negative electrode are 165 mAh/g and 330 mAh/g, respectively. Generally, the N/P ratio must be larger than 1, because, when the N/P ratio is smaller than 1,  $\text{Li}^+$  ions are easily deposited on the surface of the negative electrode, and the accumulated Li grow continuously in dendrite, penetrate the separator, and causes the internal short in the battery cell. The cell capacities are also faded out due to this dead Li. With loading balance adjusted to N/P ratio 1.2, the difference between the voltage of positive electrode and the voltage of negative electrodes is the voltage of the full cell, as described in Fig. 10 (b), which is normalized capacity from Fig. 10 (a). Fig. 10 (c) shows the charging voltage-capacity curve of the full cell, which is obtained from computer-simulated equation, which produces ‘voltage profile of full cell’ by subtracting ‘the lower voltage profile of negative electrode’ from ‘the upper voltage profile of positive electrode’, i.e. the upper voltage profile of positive electrode – the lower voltage profile of negative electrode = voltage profile of the full cell. In case that the charging voltage of full cell is cutoff at 4.2 V, the normalized capacity, which is obtained at the



intersecting point of  $V$  (Voltage) = 4.2 V, is 0.94, according to the normalized voltage-capacity graph of the Fig. 10 (d). On the normalized capacity-voltage profile of positive electrode, the specific capacity of the  $\text{LiCoO}_2$  positive electrode becomes 155 mAh/g at 0.94. Therefore, the actual charging capacity of the full cell can be predicted by multiplying the specific capacity of the positive electrode value by the actual loading weight. For example, if the loading weight is 0.11 g (electrode area of the positive electrode:  $10.8 \text{ cm}^2$ ), the charging capacity of the full cell at  $V = 4.2 \text{ V}$  can be obtained as 17 mAh by multiplying 155 mAh/g by 0.11 g.

Initial discharging capacity of a full cell is simply calculated from the following equation.

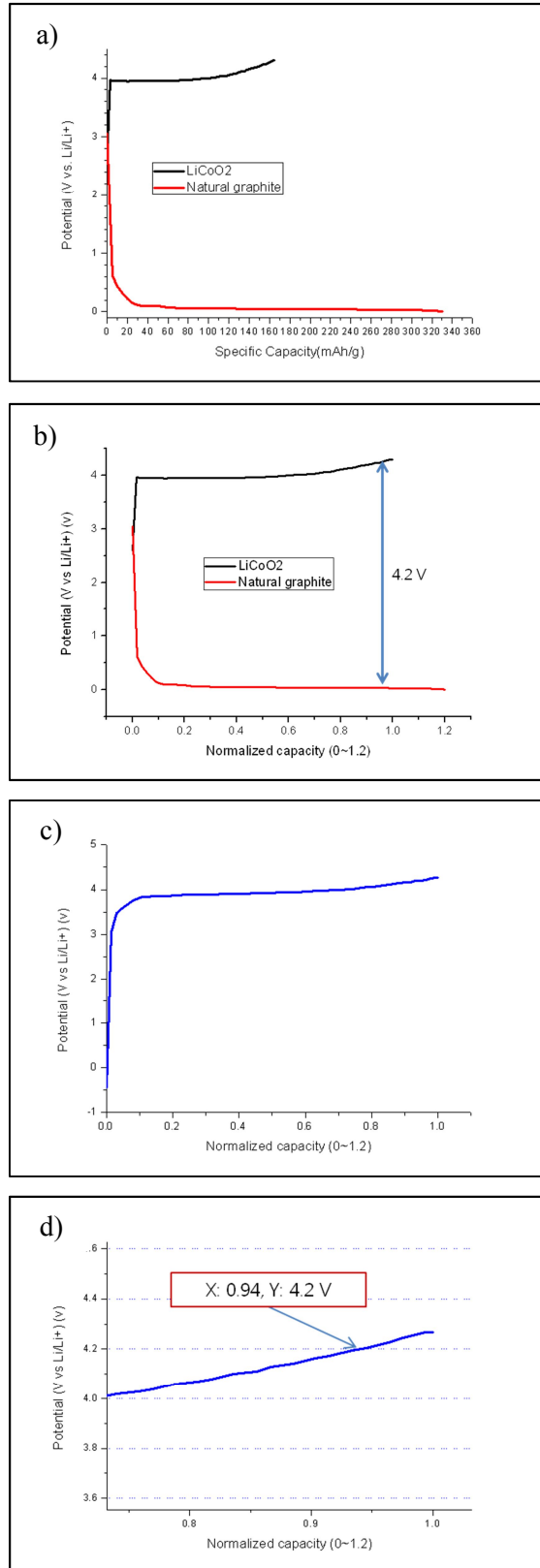
$$DC_F = CC_F - IC_A \text{-----}( 5)$$

$DC_F$  : discharging capacity of a full cell.

$CC_F$  : charging capacity of a full cell

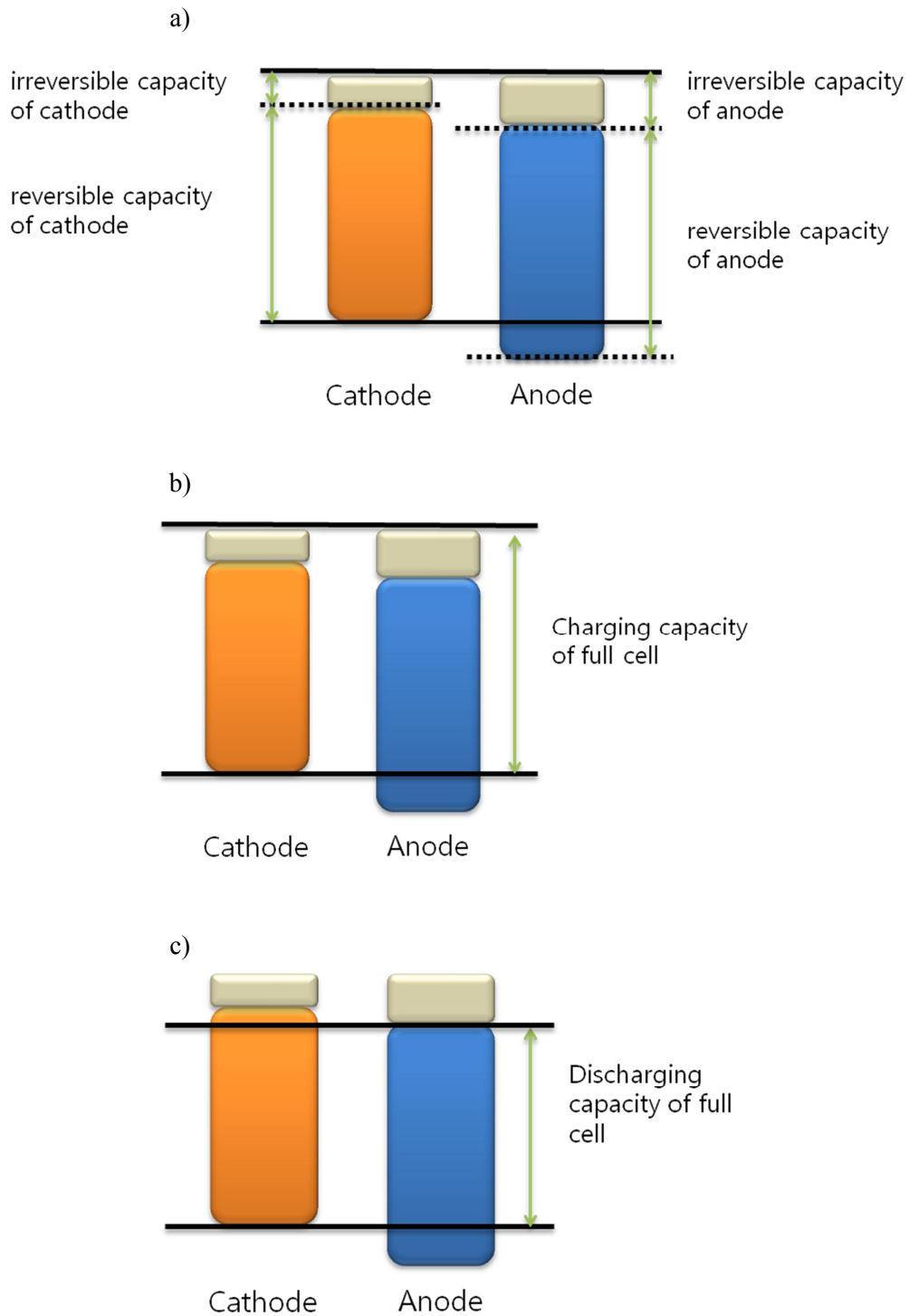
$IC_A$  : irreversible capacity of a negative electrode

Fig. 11 describes the schematic diagram of Equation 5.



**Figure 10.** Graphical views of the full cell capacity design: a) initial charge voltage profile of cathode half cell(above) and initial discharge voltage profile of anode(below) b) after loading balance (N/P=1.2) c) simulation of initial charge voltage profile of the full cell d) normalized capacity with

charging cutoff voltage 4.2 V.



**Figure 11.** Schematic views of a full cell capacity a) each reversible and irreversible capacity of cathode and anode half cell, b) charging capacity of a full cell and c) discharging capacity of a full cell.

## II. Experiments

### 2. 1. Materials

The LiCoO<sub>2</sub> based positive electrode was fabricated out of the composition of 90 wt% LiCoO<sub>2</sub> (L&F, Korea), 5 wt% Super P and 5 wt% polyvinlidene fluoride (PVdF) binder.

Negative electrode materials and its provider are listed up in table 2.

**Table 2. Active materials for negative electrode used in experiments and providers of them.**

Active materials	Provider
Spherical natural graphite	Mitsubishi (Japan)
shuttle-shaped natural graphite	LG Chem (Korea)
Porous silicon	Sejin innotech (Korea)

Negative electrodes were fabricated as follows (Table 3).

**Table 3. Composition of negative electrode and its wt %**

No	Active material(wt %)	Binder(wt %)	Note
1	spherical natural graphite(96)	SBR(2) and CMC(2)	For reference
2	porous Si(5) and spherical natural graphite(80)	SBR(8) and CMC(7)	For 400 mAh/g
3	porous Si(5) and shuttle-shaped natural graphite(80)	SBR(8) and CMC(7)	For 400 mAh/g
4	porous Si(8) and shuttle-shaped natural graphite(77)	SBR(5) and CMC(10)	For 500 mAh/g
5	porous Si(8) and shuttle-shaped natural graphite(77)	SBR(10) and CMC(5)	For 500 mAh/g
6	porous Si(8) and shuttle-shaped natural graphite(77)	PAA(10) and CMC(5)	For 500 mAh/g

Various electrolytes were prepared as follows (Table 4).

**Table 4. Electrolytes used in experiments**

No	Li salt	Solvent	Additive
1	1.15 M LiPF <sub>6</sub>	EC/ DMC/ DEC, 3/4/3 v/v	FEC 10 %
2	1.15 M LiPF <sub>6</sub>	EC/DEC, 3/7 v/v	FEC 10 %
3	1.15 M LiPF <sub>6</sub>	EC/EMC, 3/7 v/v	FEC 10 %

### 2. 2. Electrochemical measurement

Coin-type half cells (2016R-type) consisted of lithium metal as the counter electrode, a polyethylene separator and electrolytes were used for testing each positive and negative electrodes at 0.1C rate between 3.0 and 4.3 V and between 0.01 and 1.2 V, respectively. The pouch-type full cells

(electrode area is 10.8  $\text{cm}^2$  as positive electrode and 12.1  $\text{cm}^2$  as negative electrode) consisted of LiCoO<sub>2</sub> as the positive electrode, the various compositions of the mixture of porous Si and natural graphite as the negative electrode, a polyethylene separator and electrolytes.

Initial charge-discharge voltage profiles of the full cell which consisted of LiCoO<sub>2</sub> and natural graphite were obtained at a rate of 0.1 C between 3 and 4.2 V. Initial charge-discharge voltage profiles of the full cell which consisted of LiCoO<sub>2</sub> and the composite of porous Si and natural graphite as negative electrode were obtained at a rate of 0.1 C between 2.5 and 4.2 V. Full cells were charged to 4.2 V at a constant current of 0.5C, kept at 4.2 V until cutoff current 1/50 C, and discharged to each cutoff voltage at constant currents of 1 C at room temperature after initial charge-discharge(formation). The pouch type three electrode cells consisted of LiCoO<sub>2</sub> as the positive electrode, composite of porous Si and shuttle shaped natural graphite as the negative electrode, lithium metal as the reference electrode, a polyethylene separator and electrolytes.

### **2.3. Instrumental analysis**

Morphology of the samples was observed using scanning electron microscopy (SEM) (JSM 6400, JEOL). The nitrogen adsorption and desorption isotherms were measured with a VELSORP-mini II (BEL Japan, Inc.) at 77 K in the relative pressure range of  $P/P_0$  from 0.05 to 0.3 to determine the BET surface areas and size distribution. Sheet resistivity of the electrode was measured by 4 probe measurement method using AIT, CMT-SR1000N.

## **III. Results and discussion**

### **3.1 Particle size effect of natural graphite**

Fig. 12 shows the two different types of natural graphite, shuttle-shaped natural graphite (ShNG) and spherical natural graphite (SpNG), with which the effect of morphology and size of natural graphite on a silicon-based negative electrode would be investigated. The particle size and the specific surface area of ShNG are 6.29  $\mu\text{m}$  (with  $D_{90}$ ) and 19  $\text{m}^2/\text{g}$ , respectively, while the particle size and the specific surface area of SpNG are 22.30  $\mu\text{m}$  and 2  $\text{m}^2/\text{g}$ , respectively, as summarized in Table 5.

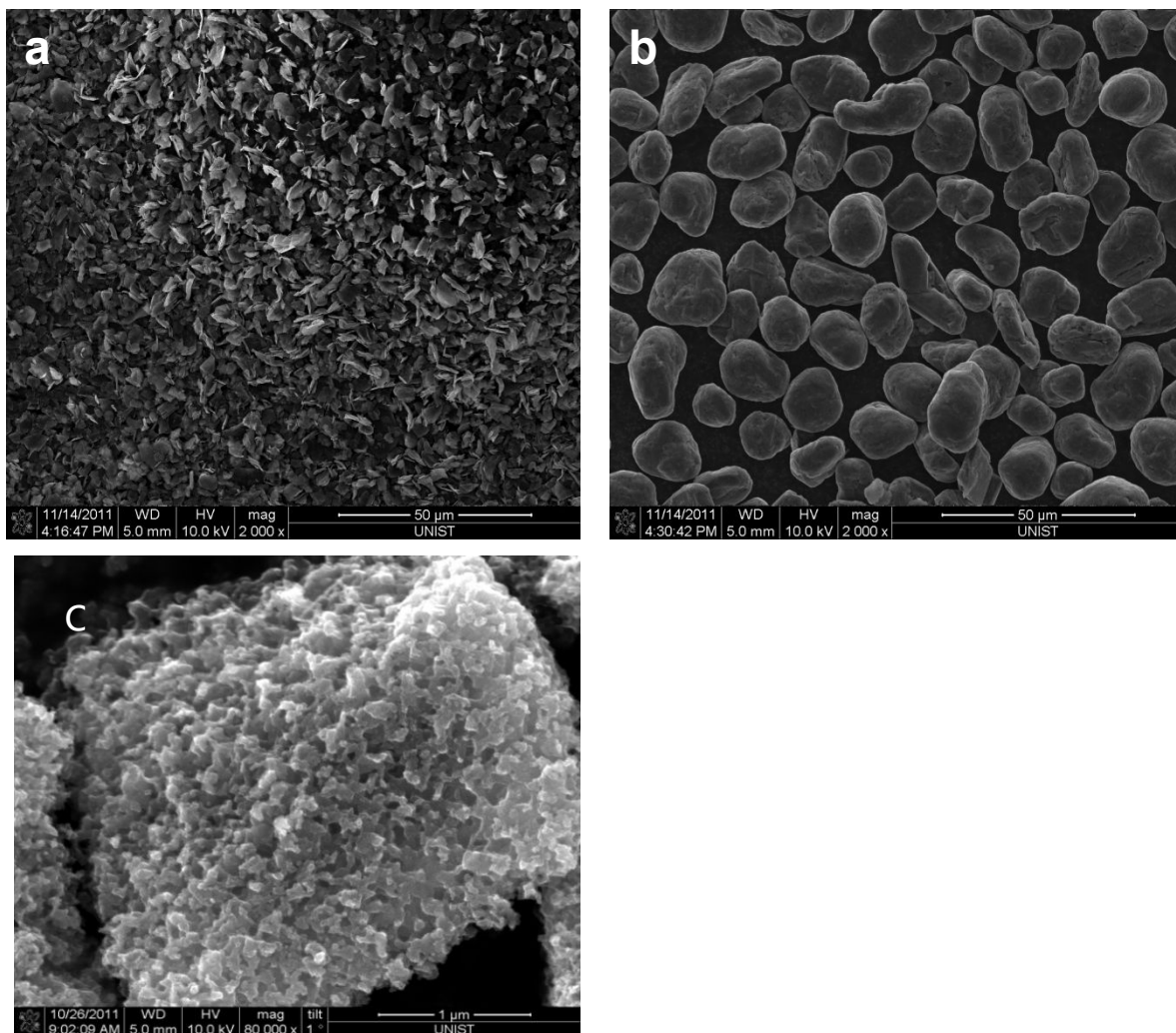


**Figure 12.** SEM image of (a) shuttle-shaped natural graphite(ShNG), (b) spherical natural graphite(SpNG) and (c) porous silicon(Si).

**Table 5. Diameter and specific surface area of each active material**

Active material	Diameter ( $\mu\text{m}$ )			BET( $\text{m}^2/\text{g}$ )
	$D_{\text{min}}$	$D_{90}$	$D_{\text{max}}$	
Shuttle-shaped natural graphite (ShNG)	2.12	6.29	11.00	19
Spherical natural graphite (SpNG)	10.09	22.30	37.00	2
Porous silicon (Si)	2.75	8.37	16.96	17

A mixture of silicon, natural graphite and binder was mixed at the ratio of 5: 80:15 by weight into a

mixture, in which the binder was composed of SBR and CMC at the ratio of 8:7 by weight. Distilled water was used as a solvent within the mixture slurry. After spread uniformly on Cu foil, the slurry was dried for 1 hour within dry oven, and then pressed to the electrode density,  $1.2 \text{ g/cm}^3$ . Finally, half cells (2016R), consisting with Li metal as the counter electrode, a polyethylene separator, and 1.15M  $\text{LiPF}_6$  in ethylene carbonate(EC),diethyl carbonate(DEC) (EC/DEC, 30:70 v/v) with 10 wt.% fluoroethylene carbonate(FEC) were assembled. Fig. 13 shows initial discharge-charge voltage profiles of the composite made of Si and ShNG (red solid line) and the composite of Si and SpNG (blue dotted line), which were obtained at 0.1C rate, with the cut-off voltages of discharge(lithiation) and charge(delithiation) at 0.01 V and 1.2 V, respectively. The discharge specific capacities of ShNG and SpNG are 530 mAh/g and 480 mAh/g, respectively, the difference of which is negligible, compared with charging voltage profile. ShNG shows another plateau at about 0.5 V range and superior coulombic efficiency with 86%, compared with 76 % of SpNG.

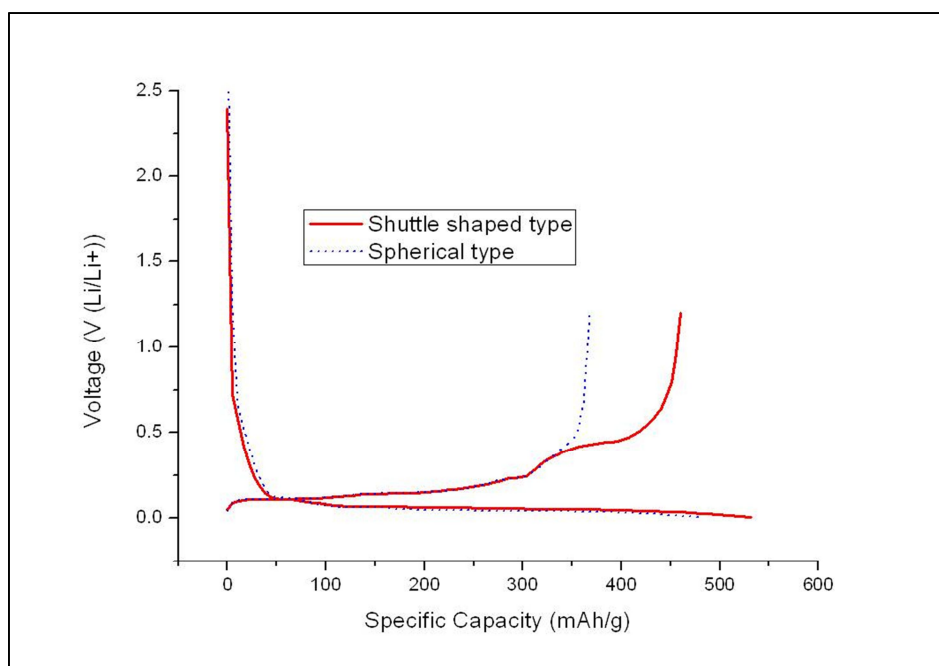


**Figure 13.** Initial discharge-charge voltage profiles (red solid line) of Si and ShNG composite and (blue dotted line) of Si and SpNG composite.

It is generally accepted that the physical- and electrochemical- properties of active material are greatly determined by particle size, specific surface area and morphology.[15, 16] From the physical aspect, it is difficult to spread uniformly the composite slurry composed of the tiny particles on the current collector, for the tiny particles are easily agglomerated due to Van der Waals force. The agglomeration phenomenon of tiny particles can also be observed at the agglomerated nano-size silicon particles, 70~80 nm, around the coarse particles of SpNG,  $\sim 22 \mu\text{m}$ , as shown in Fig. 14 (f).

In contrast, no agglomeration was observed in the mixture between coarse silicon particles,  $\sim 8.4 \mu\text{m}$ , and coarse natural graphite particles,  $\sim 22 \mu\text{m}$ , as shown in Fig. 14 (b)

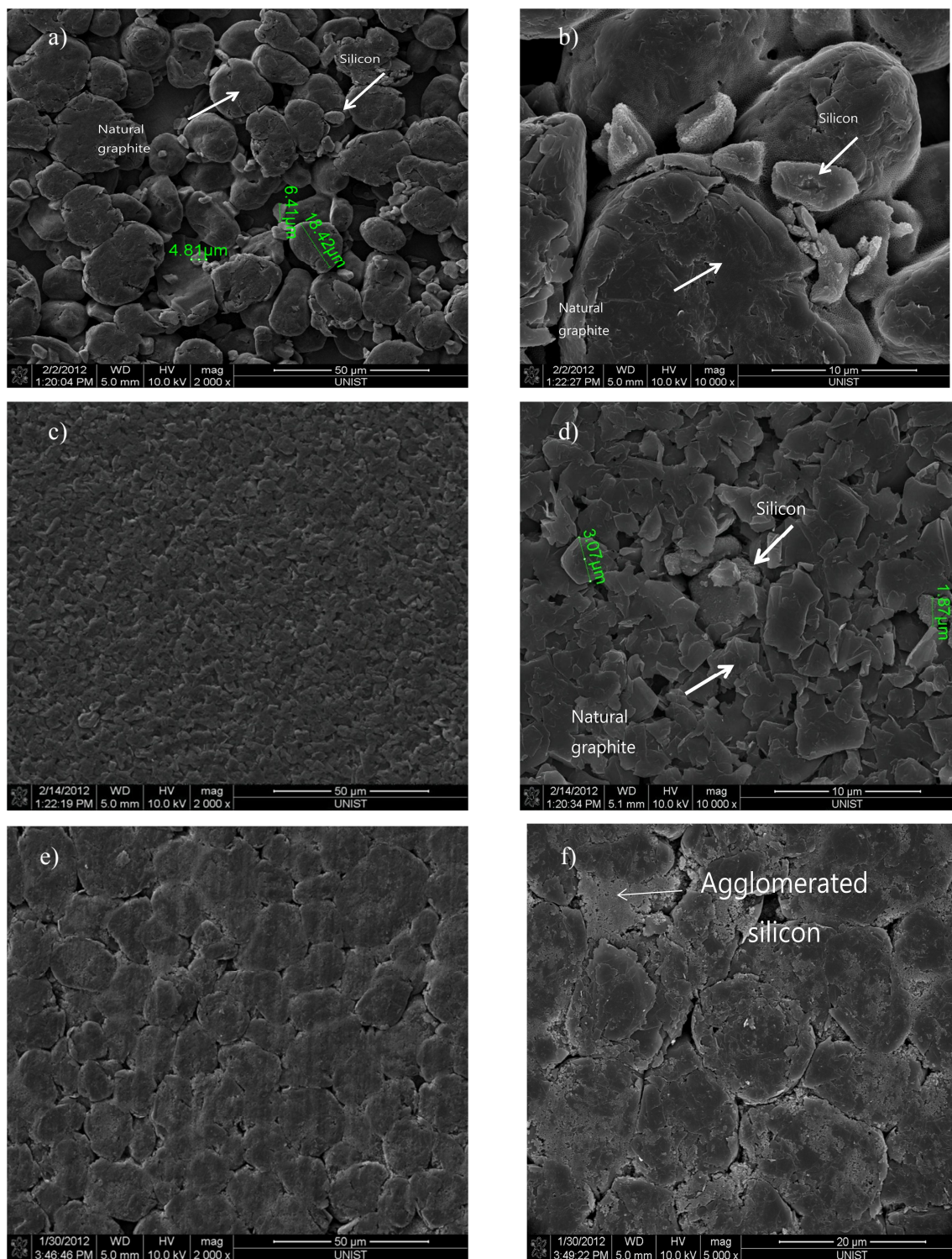


**Figure 14.** Electrode morphology of (a) Si and SpNG composite, (b) magnified SEM image of samples seen in (a), (c) Si and ShNG composite, (d) magnified SEM image of samples seen in (c), (e) nano-sized Si and ShNG composite and (f) magnified SEM image of samples seen in (e).



From the view point of electrochemistry, there are two contradictory expectations when the particle size of natural graphite decreases; one is that the intercalation of Li ions will speed up with the increasing surface area ratio of edge plane over basal plane, and the other is that electrolyte decomposition will be accelerated, forming thick solid electrolyte interface layer (SEI layer), which is also explained by the fade-out of capacity or the decrease of coulombic efficiency.[15, 16] According to the comparison profiles between coarse (SpNG, 22 $\mu$ m) and small (ShNG, 6 $\mu$ m) natural graphite particles mixed with Si in Fig. 13, small graphite particle shows higher coulombic efficiency, the result of which is contradictory to the negative expectation for the application of small graphite particles only. The higher coulombic efficiency from the mixture between small graphite particles and Si can be explained by the excellent ‘electrical conductive network’, in which the Si particles are uniformly contacted with small natural graphite particles without any isolation of Si particles. The silicon particles, which expand during charge (delithiation), are supposed to shrink to original size and isolated from the natural graphite particles which work as electrical path ways upon charge. In this case the smaller graphite particles will provide more contact points with the silicon particles, and keep the integrity of good conductive network during charge and discharge. [17]. This argument is supported by the sheet resistance values of two electrodes,  $1.11 \pm 0.01 \text{ m}\Omega/$  for coarse (SpNG, 22 $\mu$ m) and  $746 \pm 90 \text{ m}\Omega/$  for small (ShNG, 6 $\mu$ m) particles mixed with Si. Each measured electrode has the same thickness, 45 $\mu$ m, including the thickness of Cu foil, 15 $\mu$ m, which implies that this set of measurements is meaningful as comparative evaluation between these two electrodes, not as the absolute information. The higher resistance,  $746 \pm 90 \text{ m}\Omega/$ , for small (ShNG, 6 $\mu$ m) particles mixed with Si over the lower resistance,  $1.11 \pm 0.01 \text{ m}\Omega/$  for coarse (SpNG, 22 $\mu$ m) particles demonstrates that the Si particles imbedded within sample graphite particles are uniformly contacted with small natural graphite particles without any isolation of Si particles. It can be explained with 8 orders higher conductivity of graphite,  $\sim 10^4 \text{ S/cm}$ , than that of silicon,  $6.7 \times 10^{-4} \text{ S/cm}$ , contributing to for the 700 times higher sheet resistance of small (ShNG, 6 $\mu$ m) natural graphite than coarse particles, despite the low weight percent of Si, 5wt. % added into each electrode. This argument is summarized figuratively in Fig. 15.

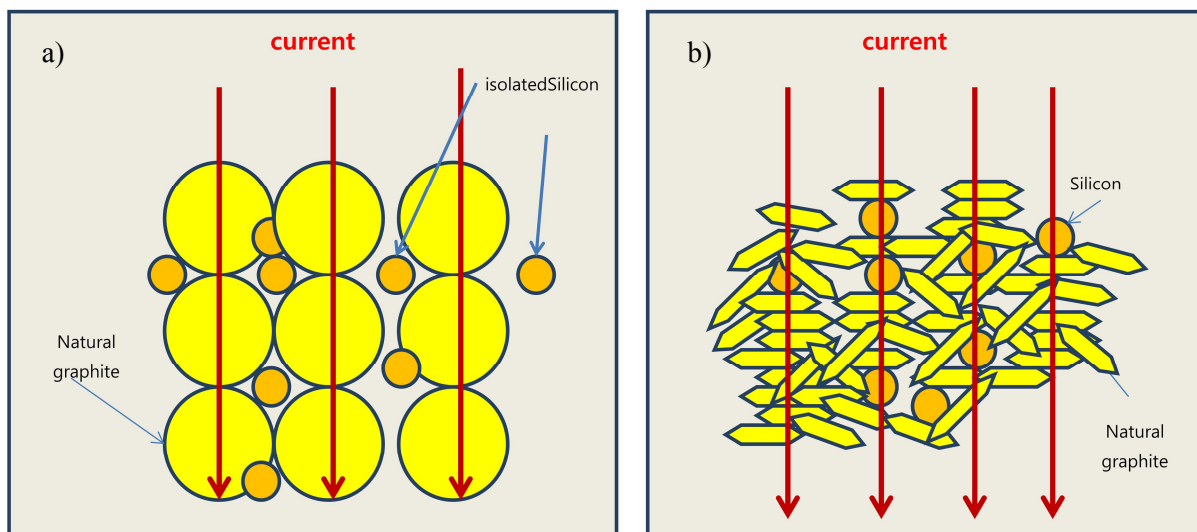


**Figure 15.** Schematic diagrams of (a) Si/ SpNG composite and (b) Si/ ShNG composite.

There is low sheet resistivity in Si/SpNG composite because most current flow the via the SpNG particles(many silicon particles are isolated from current pathway). On the other hand, composite of silicon and ShNG shows the high sheet resistivity because there are few isolated particles from current pathway. Accordingly, the electrical conductivity for composite of a silicon and natural graphite depends on the size of active material particles.

### 3.2 Design for cutoff voltage in a full cell

As has been described in normalized capacity-voltage profile between only silicon active material electrode and only SpNG active material electrode of Fig. 4 (b), while there is little difference between only silicon active material and only SpNG active material during discharge (lithiation in halfcell), silicon negative electrode shows higher voltage than natural graphite electrode during charge, Fig. 16 (b) also shows that the composite electrode between Si and ShNG show higher voltage than the only SpNG electrode during charge (delithiation in halfcell). Full cell voltage formula (full cell voltage = positive electrode voltage – negative electrode voltage) could be used for analyzing the cutoff voltage of the full cell, in which the same  $\text{LiCoO}_2$  active material was used as positive electrode, while applying different negative electrodes. In order to make the most use of the capacity of each electrode, the full cell cutoff voltage made of the composite negative electrode should be adjusted to the lower value than that made of only NG active material electrode. Fig 16 (c) shows the normalized capacity-voltage profiles (half cell) of the NG negative, the composite (Si+ShNG) negative and  $\text{LiCoO}_2$  positive electrodes, which can be replotted into the normalized capacity-voltage profile of full cell during discharge, as shown in Fig. 16 (d), by making use of full cell voltage formula (full cell voltage = positive electrode voltage – negative electrode voltage). Fig. 16 (d) shows about 0.5 V gap

between the two full cells, the full cells made of only NG negative and composite (Si+ShNG) negative electrodes at the polarization region. Therefore, while the cutoff voltage is usually set at 3.0 V during discharge in the full cell made of only NG negative, the cutoff voltage in the full cell made of composite (Si+ShNG) negative electrodes should be adjusted to 2.5 V, as a way of optimization.

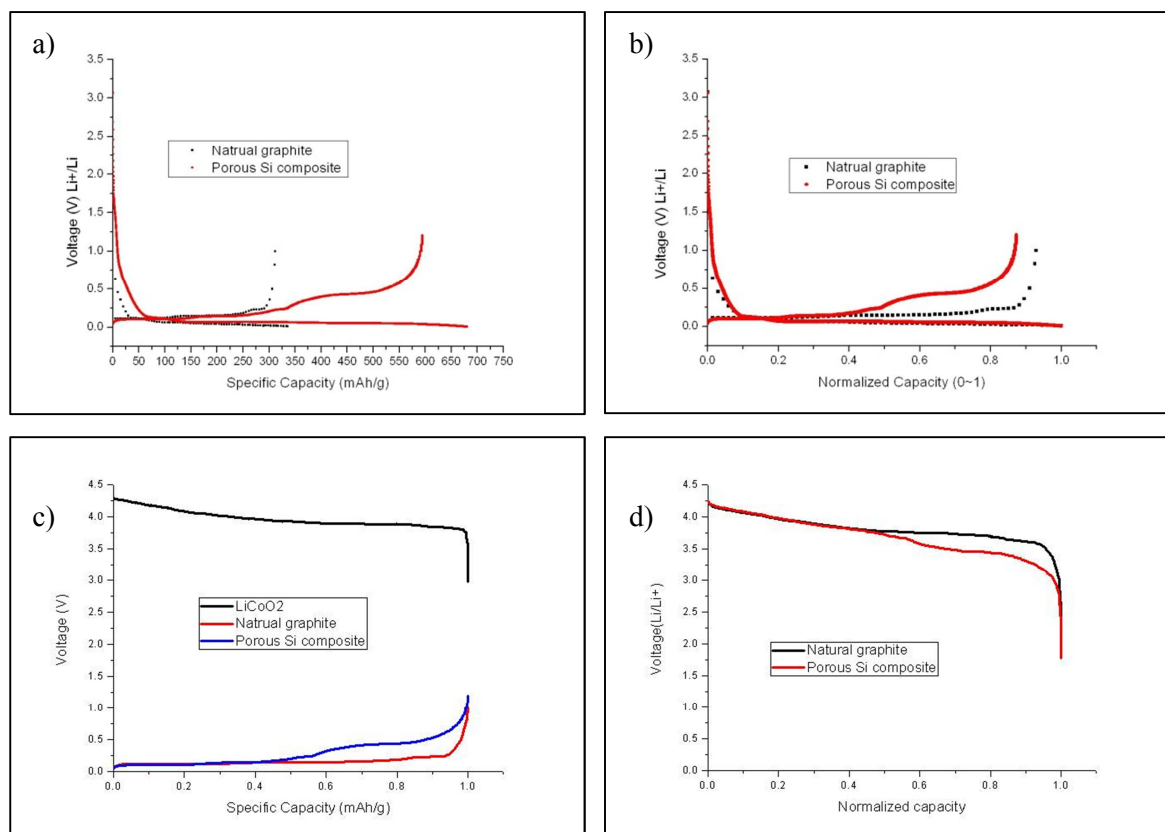


**Figure 16.** (a) Half-cell specific capacity-voltage profiles of SpNG (black dotted line) and Si/ShNG composite (red solid line), (b) half-cell normalized capacity-voltage profiles of SpNG (black dotted line) and Si/ShNG composite (red solid line), (c) half-cell normalized discharge capacity-voltage profiles of LiCoO<sub>2</sub> (black solid line), SpNG (red solid line) and Si/ShNG composite (blue solid line), (d) full cell normalized discharge capacity-voltage profiles of LiCoO<sub>2</sub>-SpNG (black solid line) and LiCoO<sub>2</sub>-Si/ShNG composite (red solid line).

### 3.3 Design for initial discharge capacity in a full cell

The proper design and estimation of the initial charge and discharge capacity within the full cell, utilizing the capacity-voltage half cell profile of each electrode, is decisive in optimizing the full cell formulation factors. In this study, a new method of designing initial discharge capacity was suggested, which was initiated by the large gap of initial discharge capacity (>4%) between design

and actual values within the full cell, compared with 2 % of initial charge capacity. The initial discharge capacity was explained by the Eq. (5).

The irreversibility of each electrode makes it difficult to predict the initial discharge capacity of the full cell, which motivated to fabricate three electrode cells consisting of negative electrode, positive electrode and lithium metal, and to study on the capacity-voltage profile, which is composed of negative electrode, positive electrode and lithium metal electrode. Fig. 17 describes the procedure of fabricating three electrodes. The charge and discharge of the full cell was executed via two terminals, positive electrode with LCoO<sub>2</sub> and the composite negative electrode with Si and ShNG, at the rate of 1/20 C.

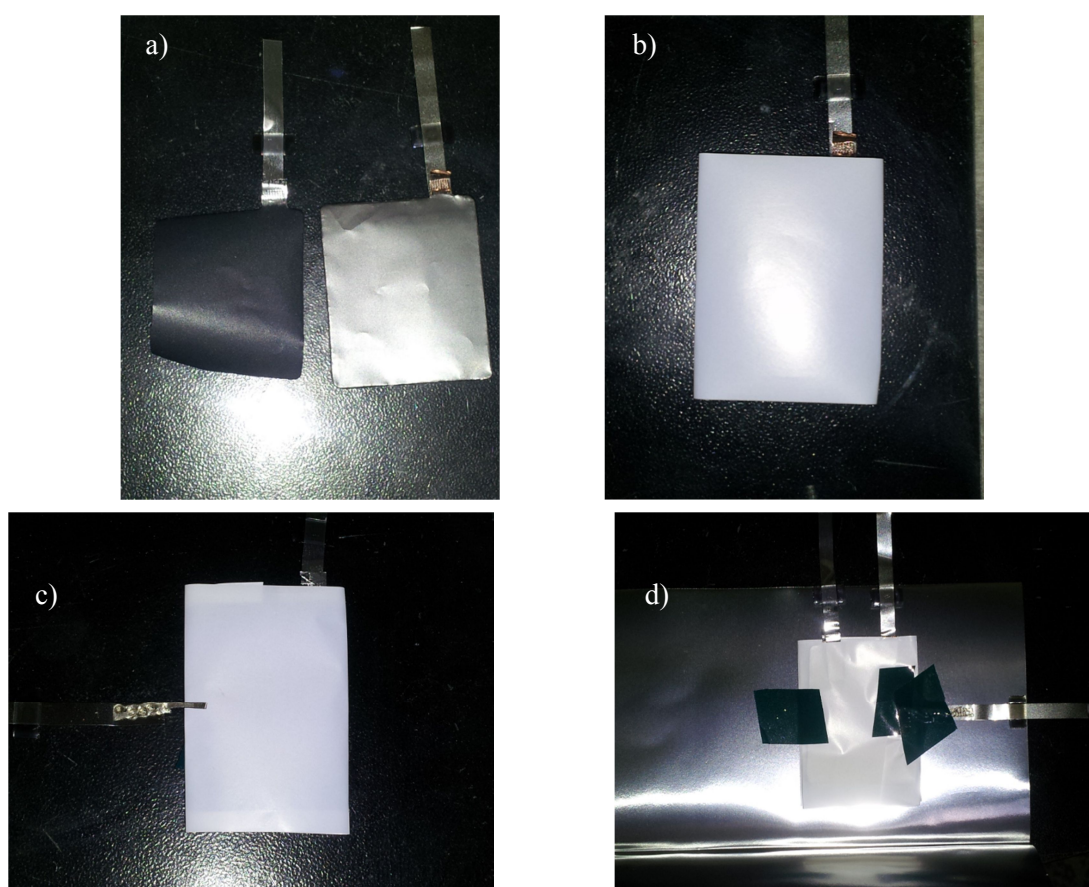


**Figure 17.** Three electrode pictures of (a) LiCoO<sub>2</sub> positive electrode(left) and Si/ShNG negative electrode(right), (b) negative electrode wrapped with separator, (c) Li metal reference electrode placed between positive electrode and negative electrode and (d) pouch type three electrode.

According to capacity-voltage profiles of the Fig. 18 (a), it is possible to read simultaneously the voltage changes of negative electrode/Li metal and positive electrode/Li metal in Fig. 17 (d), while observing the charge and discharge of the full cell. The profiles of Fig. 18 (a) shows that the polarization of the full cell during discharge is dependent on negative electrode, which is coincident

with the description of equation (5), where the discharge capacity of the full cell is determined by the irreversibility of the negative electrode. The positive electrode, with 1.2 of the NP ratio, rarely affects the discharge polarization of the full cell, which is manifested by the simulated capacity-voltage profile of the positive electrode by making use of the half cell data of the positive electrode, as shown in Fig. 18 (b).

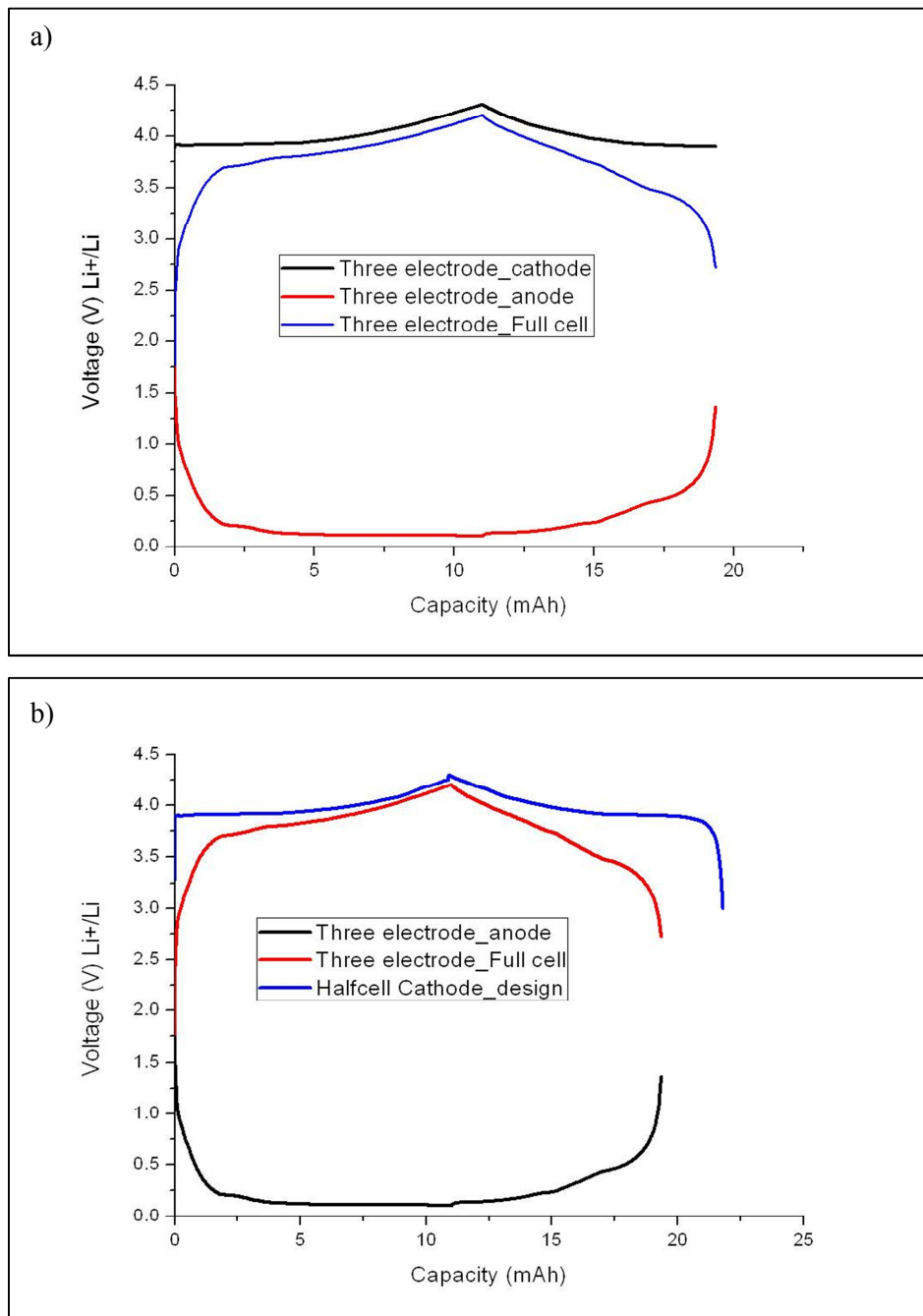


**Figure 18.** Three electrode voltage profiles of LiCoO<sub>2</sub> positive electrode voltage profile(upper) , full cell voltage profile(middle) and Si/ShNG negative electrode(below); (a) actual three electrode voltage profiles, (b) three electrode voltage profiles (simulated positive electrode voltage profile is substituted with actual positive electrode voltage profile).

However, when different sets of samples were tested to predict the initial discharge capacities of full cells by accommodating equation (5), there is above 4 % of deviation between actual and design values. The repeated experimental results herald that the initial discharge capacities of full cells are determined not only by the irreversibility of the negative electrode but also that of the positive electrode, as summarized in Table 6. When the initial irreversible capacities of both the negative and positive electrodes are obtained by the initial coulombic efficiency of each half cell, the initial discharge capacities of full cell are calculated by subtracting the initial irreversible capacities of both the negative and positive electrodes from the initial charge capacity of the full cell, where there is no significant difference between the design and the actual values in Table 6.

**Table 6. Design and actual values of full cell capacity**

(Positive electrode: LiCoO<sub>2</sub>, Negative electrode: Natural graphite, 0.1 C charge-discharge, Cutoff voltage: (3.0 ~ 4.2) V)

No	N/P ratio	Design value (mAh)				Actual value (mAh)		Error of discharge capacity (%)
		Charge capacity	Irreversible capacity of negative electrode	Irreversible capacity of positive electrode	Discharge capacity	Charge capacity	Discharge capacity	
1	1.04	17.0	1.4	0.7	<b>14.9</b>	17.2	<b>15.1</b>	1
2	1.38	16.3	1.8	0.7	<b>13.9</b>	16.3	<b>14.1</b>	1
3	1.41	15.5	1.8	0.6	<b>13.1</b>	15.3	<b>13.1</b>	0

On the base of more realistic experimental result of our investigation, we can suggest that the initial discharge capacity should be calculated out of the modification of equation (5) as follows,

$$DC_F = CC_F - IC_A - IC_C \text{-----( 6)}$$

DC<sub>F</sub> : discharging capacity of full cell.

CC<sub>F</sub> : charging capacity of full cell

IC<sub>A</sub> : irreversible capacity of negative electrode

$IC_C$  : irreversible capacity of positive electrode

### 3.4 Optimization of binder and electrolyte

Generally, natural graphite negative electrode for commercial application consists of a binder mixture between SBR and CMC. As has been mentioned above in the introduction, it is reported that CMC has chemical bonding, which makes it as a strong candidate of binder for the silicon based negative electrode which is greatly expansive during lithiation, in spite of its high stiffness and small deformation range. [12, 13, 18]. In order to confirm the effect of CMC as a binder in the silicon based negative electrode, the cell performance was evaluated by changing the weight ratio between SBR, CMC, 5:10 and 10:5, within the compositional ratio of 8: 77:15 for silicon: ShNG:binder.

As a way of figuring out which factor is critical in cell performance and understanding the interaction effect among binder ratio, electrode density and electrolyte, a statistical method, Design of Experiment (DOE), was applied for analysis. Table 7 is the list of levels and values of each factor, which are assorted and combined into 8 different experimental conditions of 2016 coin-typed half cell, as described in Table 8. Cell performance was evaluated according to two characteristics, specific discharge capacity(delithiation) and initial coulombic efficiency, the results of which are also summarized in Table 8. The key factor and the interaction effect among the experiment result in Table 8 were determined by making use of a statistical program, Minitab.

**Table 7. Factorial design of suspicious factors on the cell performance**

Factor	Level	
	Low (-1)	High (+1)
Electrode density (g/cm <sup>3</sup> )	0.8	1.2
Composition ratio of binders (wt %)	SBR:CMC = 5:10	SBR:CMC= 10:5
Electrolyte (v/v )	EC/DEC=3:7 + FEC 10%	EC/EMC=3:7+ FEC 10%

**Table 8. Full factorial design and its results**

Electrode Density(g/cm <sup>3</sup> )	Binder (SBR:CMC wt%)	Electrolyte (with 1.15 M LiPF <sub>6</sub> )	Discharge Capacity (mAh/g)	Initial C.E. (%)
0.8	5:10	EC:DEC=3:7,+FEC10%	470	85
1.2	5:10	EC:DEC=3:7,+FEC10%	432	83
0.8	10:5	EC:DEC=3:7,+FEC10%	402	82
1.2	10:5	EC:DEC=3:7,+FEC10%	490	81
0.8	5:10	EC:EMC=3:7,+FEC10%	470	83
1.2	5:10	EC:EMC=3:7,+FEC10%	581	85
0.8	10:5	EC:EMC=3:7,+FEC10%	520	79
1.2	10:5	EC:EMC=3:7,+FEC10%	561	80

The analysis result shows that the most determinant factor in the performance of initial specific discharge capacity was electrolyte, which was confirmed by 0.043 of p-value within the analysis of variance Table 9 (a), in which any p-value below 0.05 is a significant factor. When the half cell, making use of an electrolyte (EC:EMC=3:7 v/v, +FEC 10%), was applied, the average initial specific discharge capacity was 533 mAh/g, which was 84.5 mAh/g higher than that made of the other electrolyte (EC:DEC=3:7 v/v, +FEC 10%). Such a higher average initial specific discharge capacity by applying the electrolyte (EC:EMC=3:7 v/v, +FEC 10%) as key factor was also certified in the main effects plot of Fig. 19 (a). The highest slope of capacity against factor is decided as the key factor of the initial specific discharge capacity as shown in Fig. 19 (a) The other cell performance, initial coulombic efficiency, is affected by the weight ratio changes of a mixture binder between SBR:CMC, in which the p-value of binder factor was 0.035. When the weight ratio of SBR:CMC was 5:10, the average initial coulombic efficiency was 84 %, showing 3 % higher than that made at the weight ratio of 10:5 between SBR:CMC. There was no interactive effect among factors that the two cell performances. In short, cell performance is decided by main effects of binder and electrolytes.

In consideration of binder effect only, this study proves that CMC is superior to SBR in the silicon based negative electrode, which coincides with other reports. [12, 13]



**Table 9.** Analysis of variance for initial specific discharge capacity and coulombic efficiency.

Estimated Effects and Coefficients for Discharge Capa (coded units)					
Term	Effect	Coef	SE Coef	T	P
Constant		490.750	14.46	33.93	0.000
Electrode Density	50.500	25.250	14.46	1.75	0.156
Binder	5.000	2.500	14.46	0.17	0.871
<b>Electrolyte</b>	<b>84.500</b>	<b>42.250</b>	<b>14.46</b>	<b>2.92</b>	<b>0.043</b>

a) Analysis of variance for initial specific discharge

Estimated Effects and Coefficients for Initial C.E. (coded units)					
Term	Effect	Coef	SE Coef	T	P
Constant		0.82328	0.005299	155.36	0.000
Electrode Density	-0.00213	-0.00107	0.005299	-0.20	0.850
<b>Binder</b>	<b>-0.03327</b>	<b>-0.01664</b>	<b>0.005299</b>	<b>-3.14</b>	<b>0.035</b>
Electrolyte	-0.00993	-0.00496	0.005299	-0.94	0.402

(b) Analysis of variance of initial coulombic efficiency

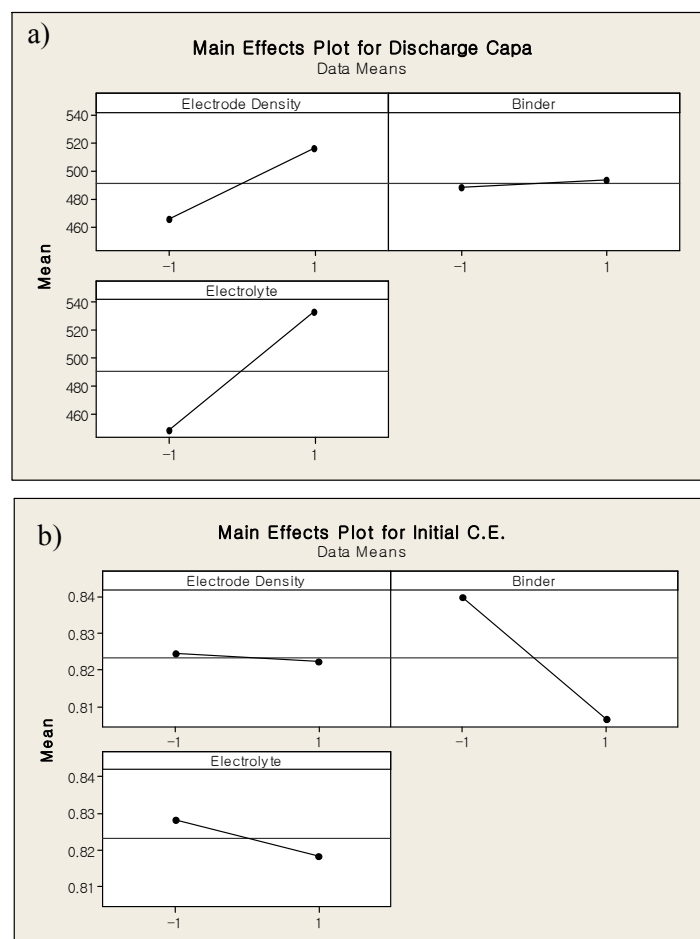


**Figure 19.** Main effect plots of (a) initial specific discharge capacity and (b) initial coulombic efficiency.

The superior cycling stability in the cell made of CMC to that of SBR or PVDF is usually attributed to chemical bonding, despite its high stiffness.[12, 13, 14] , in which the total deformation capacity of that made of CMC is low. However, it is generally well known that the elastic deformation capacity contributes more critically to recovering a material to original size after its expansion in the linear region of Strain-Stress diagram of Fig. 6 (b). In case strain passes over proportional limit stress of the linear region, it enters into plastic deformation and cannot recover to its original size, as described in Fig. 6 (b). So, the expansion of any active material should be allowed within the elastic deformation of any binder in order to maintain electrical conductive network, which was schematically summarized in Fig. 20.

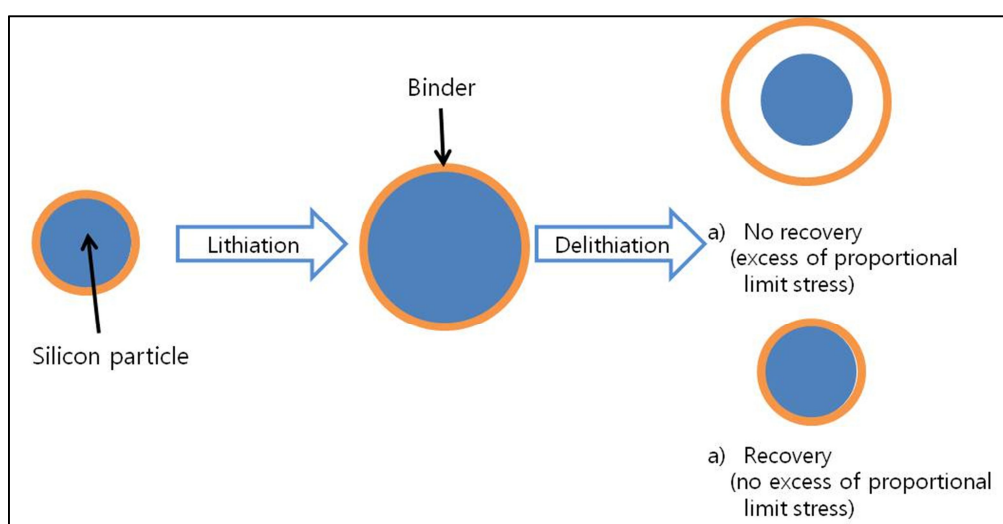


**Figure 20.** Schemetic diagram of plastic deformation and elastic deformation.

According to the S-S diagram of Fig. 6 (a), the proportional limit stress and proportional limit strain are estimated to be 13 MPa and 4 %, respectively, for PVDF, and 20 MPa and 1 %, respectively, for CMC. And, the proportional limit stress of SBR is considered to be smaller than that of CMC, on the ground that CMC/SBR is located between CMC and PVDF curves within the S-S diagram.[12] This denotes that, when SBR is used within the silicon based negative electrode, the deficiency of chemical bonding and the low proportional limit stress give rise to plastic deformation during silicon expansion, for the expansion stress of silicon particles during lithiation will pass over the proportional limit stress of SBR.

The cycle life of the full cell was evaluated, as a way of verifying the optimized binder and electrolyte in the full cell, which were already confirmed in the half cell. The active material of positive electrode was  $\text{LiCoO}_2$ , the electrode of which is composed of the weight ratio of 90:5:5 for  $\text{LiCoO}_2$ :Super-p:PVDF. The active material of negative electrode was a composite between silicon and ShNG, the electrode of which is composed of two different weight ratios of 8:77:5:10 and

8:77:8:7 for Si/ShNG:SBR:CMC. In pursuit of figuring out additionally the effect of the electrolyte on the positive electrode, while the electrolyte was optimized in the half cell of negative electrode, three different kinds of electrolytes including EC:EMC=3:7,+FEC10% were applied in the study of the full cell system, as has been described in Fig. 21. The cycle life experiment was executed by 0.5C during charge and 1C during discharge between 4.2 and 2.5V, after 0.1C formation.

As for the survey on the binder effect, Fig. 21 shows that the cycle life of the full cell at SBR:CMC=5:10 is superior to SBR:CMC=8:7 under the same electrolyte, EC:DMC:DEC=3:4:3 v/v + FEC 10 %, the result of which is coincident with the enhancement of initial coulombic efficiency in the negative electrode half cell with the increase of CMC percentage, as shown in Fig. 19 and Table 9.

From the viewpoint on the effect of different electrolytes in the full cell, while using the same weight ratio of negative electrode of 8:77:5:10 for Si:ShNG:SBR:CMC, the same electrolyte of EC:EMC=3:7,+FEC10%, which were superior discharge capacity in the negative electrode half cell, showed the most outstanding result in the full cell.

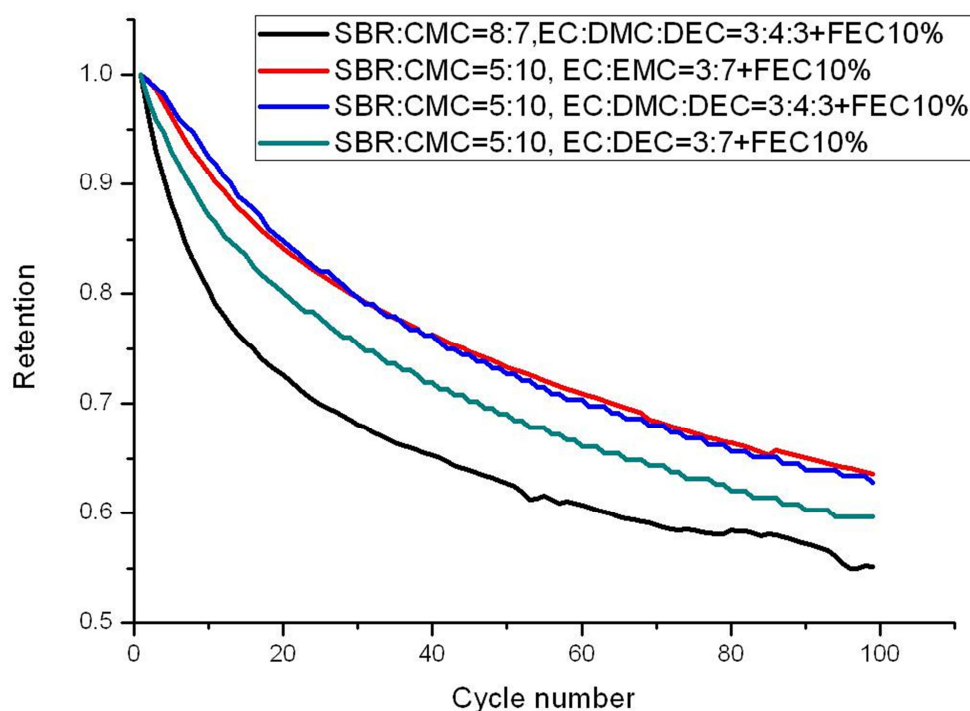


**Figure 21.** Full cell cycle life with normalized capacity after 0.1 C formation (0.5 C charging, 1 C discharging, 4.2~2.5 V cutoff).

**Table 10. Cycle life of the full cell made of different electrolyte and weight ratio of binder mixture.**

N/P	Binder (SBR:CMC wt%)	Electrolyte (with 1.15 M LiPF <sub>6</sub> , v/v %)	100 Cycle Retention (%)	Note
1.15	5:10	EC:DMC:DEC=3:4:3,+FEC10%	62	Fig 14 a) Blue solid line
1.10	5:10	EC:EMC=3:7,+FEC10%	64	Red solid line
1.11	5:10	EC:DEC=3:7,+FEC10%	59	Cyan solid line
1.20	8:7	EC:DMC:DEC=3:4:3,+FEC10%	55	Black solid line

Fig. 21 and Table 10 show that the highest the retention of cycle life in the full cell is 64% when the optimized electrolyte and binder, EC:EMC=3:7,+FEC10% and SBR:CMC = 5:10, respectively, were used. However, the retention value, 64%, is far lower than that of the commercialized full cell, 92%, the experiment of which was executed in the lab making use of the commercialized active materials, LiCoO<sub>2</sub> and natural graphite as shown in Fig. 22.

As an effort of catching up with the performance of the commercialized full cell, another binder system, PAA:CMC, instead of that of SBR:CMC, was applied after the report of Choi et al. [14], by making use of the weight ratio of 8:77:10:5 for Si:ShNG:PAA:CMC for the negative electrode in the full cell. The result showed 73% of retention for the application of the PAA:CMC, 9% higher than that of the previous SBR:CMC, as shown in Fig. 22. Choi et al. reported that cross linked PAA/ CMC binder showed with high proportional limit stress and low proportional limit strain in the Stress-Strain diagram, which confirm the previous argument that the expansion of any active material should be allowed within the elastic deformation of any binder in order to maintain electrical conductive network, which was schematically summarized in Fig. 20.

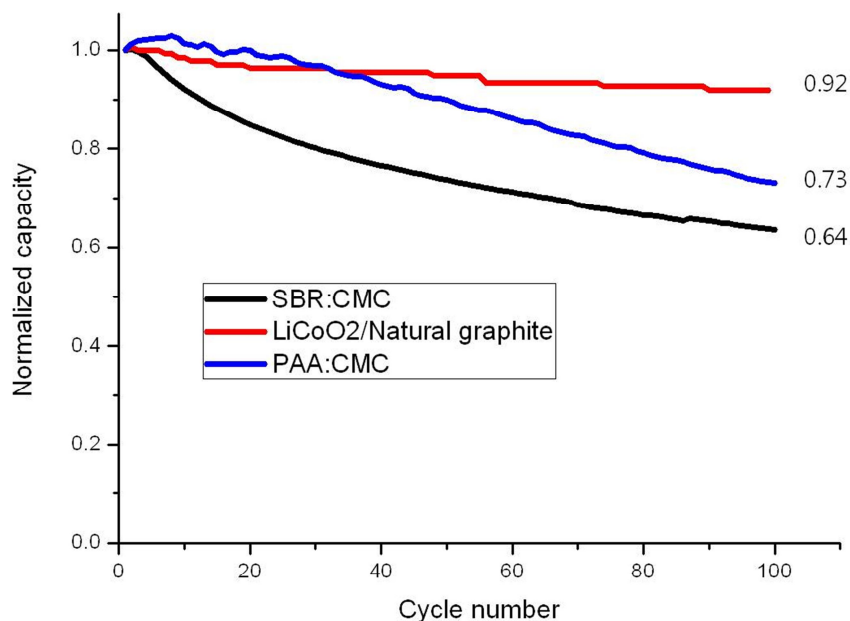


**Figure 22.** Full cell cycle life with normalized capacity after 0.1 C formation: (red solid line) LiCoO<sub>2</sub>/SpNG, (blue solid line) LiCoO<sub>2</sub>-Si/ShNG with PAA and CMC binder, and (black solid line) LiCoO<sub>2</sub>-Si/ShNG with SBR and CMC binder.

The retention value, 73%, with the application of cross linked PAA/CMC is still behind of the commercialization. The performance of cycle life in the full cell could not be improved enough due to the pulverization of the silicon particles, though there have been various efforts; minimization of natural graphite size in the composite, the control of cutoff voltage and optimization of binder system, where the weight ratio of the negative electrode in the full cell is 8:77:10:5 of Si, ShNG:PAA:CMC and specific capacity was set at 500 mAh/g during charge (delithiation).

The high gravimetric capacity of the negative electrode in the full with the specific capacity above 500 mAh/g still remains as a challenge.

## IV. Conclusions

On the base that battery performance depends significantly on the electrode formulation engineering, the optimization of the composition of active materials, binders, electrolytes and full cell cutoff voltage in silicon based electrode was investigated in this study.

Small natural graphite particles formed excellent electrical conductive network with silicon particles, contributing to the enhancement of the capacity and coulombic efficiency.

A full cell cutoff voltage should be adjusted according to different active materials; as the silicon based composite electrode keeps higher voltage profile than that of natural graphite, especially during delithiation in the half cell, the cutoff voltage in the full cell should be shifted to the lower voltage during discharge in the full cell consisting of silicon–natural graphite composite electrode in order to use the maximum capacity of each electrode.

This study suggest that, for the sake of designing full cell initial capacity, the initial charge capacity in the full cell should be estimated out of the initial charge capacity at the positive electrode in the half cell, and, on the other hand, the initial discharge capacity in the full cell should be estimated by subtracting the irreversible capacities of both electrodes from the obtained initial charge capacity in the full cell.

Those binders, which have mechanically high ‘proportional limit stress’ like PAA and CMC, provide more excellent cycle life to the full cell with negative electrode composite mixed between silicon and natural graphite, because of the excellent electrical conductivity of a composite negative electrode despite under repeated dimensional changes during cycles, which are comparable with SBR and PVDF which have low ‘proportional limit stress’.

In spite of these sequent efforts of optimization, there still remains as a challenge to apply silicon based negative electrode in the commercialized products towards the high specific capacity over 500 mAh/g.

## V. References

1. Yoshio, M., T. Tsumura, and N. Dimov, *Electrochemical behaviors of silicon based anode material*. Journal of Power Sources, 2005. **146**(1-2): p. 10-14.
2. Chan, C.K., et al., *High-performance lithium battery anodes using silicon nanowires*. Nature Nanotechnology, 2008. **3**(1): p. 31-35.
3. Park, M.H., et al., *Silicon Nanotube Battery Anodes*. Nano Letters, 2009. **9**(11): p. 3844-3847.
4. Kim, H., et al., *Three-Dimensional Porous Silicon Particles for Use in High-Performance Lithium Secondary Batteries*. Angewandte Chemie-International Edition, 2008. **47**(52): p. 10151-10154.
5. Bang, B.M., et al., *High-Performance Macroporous Bulk Silicon Anodes Synthesized by Template-Free Chemical Etching*. Advanced Energy Materials, 2012. **2**(7): p. 878-883.
6. Jia, H., et al., *Novel Three-Dimensional Mesoporous Silicon for High Power Lithium-Ion Battery Anode Material*. Advanced Energy Materials, 2011. **1**(6): p. 1036-1039.
7. Zhao, X., et al., *In-Plane Vacancy-Enabled High-Power Si-Graphene Composite Electrode for Lithium-Ion Batteries*. Advanced Energy Materials, 2011. **1**(6): p. 1079-1084.
8. Lee, J.H., et al., *Spherical silicon/graphite/carbon composites as anode material for lithium-ion batteries*. Journal of Power Sources, 2008. **176**(1): p. 353-358.
9. Xu, K., *Nonaqueous liquid electrolytes for lithium-based rechargeable batteries*. Chemical Reviews, 2004. **104**(10): p. 4303-4417.
10. Yoshio, M., et al., *Improvement of natural graphite as a lithium-ion battery anode material, from raw flake to carbon-coated sphere*. Journal of Materials Chemistry, 2004. **14**(11): p. 1754-1758.
11. Lestriez, B., *Functions of polymers in composite electrodes of lithium ion batteries*. Comptes Rendus Chimie, 2010. **13**(11): p. 1341-1350.
12. Li, J., R.B. Lewis, and J.R. Dahn, *Sodium carboxymethyl cellulose - A potential binder for Si negative electrodes for Li-ion batteries*. Electrochemical and Solid State Letters, 2007. **10**(2): p. A17-A20.
13. Bridel, J.S., et al., *Key Parameters Governing the Reversibility of Si/Carbon/CMC Electrodes for Li-Ion Batteries†*. Chemistry of Materials, 2010. **22**(3): p. 1229-1241.
14. Koo, B., et al., *A Highly Cross-Linked Polymeric Binder for High-Performance Silicon Negative Electrodes in Lithium Ion Batteries*. Angewandte Chemie International Edition, 2012. **51**(35): p. 8762-8767
15. Zaghib, K., et al., *Effect of particle morphology on lithium intercalation rates in natural graphite*. Journal of Power Sources, 2003. **124**(2): p. 505-512.

16. Liu, W.R., et al., *Effect of electrode structure on performance of Si anode in Li-ion batteries: Si particle size and conductive additive*. Journal of Power Sources, 2005. **140**(1): p. 139-144.
17. Ryu, J.H., et al., *Failure modes of silicon powder negative electrode in lithium secondary batteries*. Electrochemical and Solid State Letters, 2004. **7**(10): p. A306-A309.
18. Lestriez, B., et al., *On the binding mechanism of CMC in Si negative electrodes for Li-ion batteries*. Electrochemistry Communications, 2007. **9**(12): p. 2801-2806.



## VI. Thanks to

회사생활을 하다가 늦깎이로 배터리 분야에 입문하게 되어, 공부하라, 실험하라 2년여 시간이 쏠살같이 지나간 것 같습니다. 생애 전환기의 나이에 새로운 학문에 도전하기란 쉬운 일이 아니었지만, 대학원의 많은 분들 도움으로 무사히 석사과정을 마칠 수 있게 된 거 같습니다. 특히 논문주제를 풀셀 설계로 권고해주시고 지도해 주신 조재필 교수님 덕분에 배터리 구성 요소에 대해 전반적으로 이해할 수 있게 되었던 좋은 기회가 된 것 같습니다. 다시 한번 감사의 인사 드립니다. 그리고 저의 논문작성에 도움 주신 정재일 박사님, 실험에서 풀셀 설계 및 삼전극 실험에 도움 준 조용현 박사, 이상한 학생에게 감사의 말 전합니다. 학기초, 그룹 스터디를 통하여 따라가기 힘들었던 교과과정을 무사히 마칠 수 있도록 도움 준 정수경 학생에게도 고맙게 생각합니다. 그 외 많은 분들이 자신의 지식과 경험을 기꺼이 공유하여 저에게 많은 가르침을 주었지만, 지면을 통해 일일이 열거할 수 없음을 죄송하게 생각합니다.

석사과정 동안 일정부분 학문적 성취를 이루었다고 생각하지만, 공부란 것이 배울수록 본인의 미진함을 느끼게 하는 것 같습니다. 하지만, 회사 안 울타리에서는 겪어보지 못할 경험과 젊은 문화 또한 많이 배우고 가길래 아쉬움을 뒤로 하고 졸업합니다.

석사 과정에서 배우고 경험하였던 이 모든 것들이 저의 인생 후반 열정적으로 회사생활을 할 수 있는 동력이 될 것이라 확신하며 이 글을 마칩니다.

2013년 2월 17일 석사 정성원 올림.